European Journal of Medicinal Chemistry 297 (2025) 117970

Contents lists available at ScienceDirect

European Journal of Medicinal Chemistry

journal homepage: www.elsevier.com/locate/ejmech

Research paper

Highly effective Ru(II) and Os(II) half-sandwich complexes induce cytotoxicity in cancer cells through combined mitochondrial and endoplasmic reticulum stress

Jan Hošek [a,*], Kamila Petrželová [b], Renata Héžová [a], Nicol Straková [a], Simona Kajabová [a], Ivan Nemec [b], Pavlína Šimečková [a], Kateřina Pěnčíková [a], Josef Mašek [a], Ján Moncoľ [c], Pavel Štarha [b,**]

[a] Department of Pharmacology and Toxicology, Veterinary Research Institute, Hudcova 296/70, Brno, 62100, Czech Republic
[b] Department of Inorganic Chemistry, Faculty of Science, Palacky University Olomouc, 17. listopadu 12, 77146, Olomouc, Czech Republic
[c] Department of Inorganic Chemistry, Faculty of Chemical and Food Technology, Slovak University of Technology in Bratislava, Bratislava, SK-81237, Slovakia

ARTICLE INFO

Keywords:
Ruthenium
Osmium
Antiproliferative activity
Stress gene expression
Endoplasmic reticulum
Mitochondria

ABSTRACT

A series of ruthenium(II) and osmium(II) half-sandwich complexes was synthesized and characterized for its potential as a new class of anticancer agents. The complexes feature polycyclic aromatic hydrocarbon (PAH)-substituted Schiff bases and were rationally designed to combine the redox-modulating MoA of half-sandwich Ru, Rh, Os and Ir complexes, connected with their ability to induce the formation of various reactive oxygen species (ROS), with the ability of PAH-substituents to target and disrupt DNA. The complexes [Ru(η^6-pcym)Cl(L)]PF_6 (**1**–**4**) and [Os(η^6-pcym)Cl(L)]PF_6 (**5**–**8**) were stable in aqueous environments, in contrast to the rapid degradation observed for the co-studied rhodium(III) (**9**–**12**) and iridium(III) (**13**–**16**) [M(η^5-Cp*)Cl(L)]PF_6 complexes; L = ethane-1,2-diamine-based Schiff bases (L1–L4) bearing two terminal PAH substituents 2-naphtyl (for L1), 9-anthracenyl (for L2), 9-phenanthrenyl (L3) or 1-pyrenyl (L4); pcym = 1-methyl-4-(propan-2-yl)benzene (*p*-cymene), Cp* = pentamethylcyclopentadienyl. Biological testing demonstrated that **1**–**8** possess significant antiproliferative activity against various lung cancer cell lines, including those resistant to cisplatin, with Os(II) complex **5** showing the highest cytotoxicity. Treatment with these complexes led to the activation of stress-related gene pathways, including unconventional endoplasmic reticulum stress, apoptotic signalling, and mitochondrial membrane depolarization. Activation of p21/GADD45A pathway indicates DNA-damage response, as well. Notably, these complexes did not induce significant inflammatory responses, a notable advantage over cisplatin. The results highlight the potential of Ru and Os half-sandwich complexes as alternative metallodrugs, capable of overcoming platinum resistance and minimizing inflammatory side effects. This study suggests that these compounds could serve as a promising class of anticancer agents for future clinical development.

1. Introduction

Lung cancer represents one of the most dangerous cancer types. Two main types of lung cancer can be distinguished - small cell lung cancer (SCLC) and non-small cell lung cancer (NSCLC), with SCLC being more aggressive and typically diagnosed at a later stage. [1,2]. In terms of incidence, lung cancer is one of the most frequently newly diagnosed cancers (3rd in incidence) and the most common cause of cancer deaths (over 20 % of all cancer-related deaths) [3–5]. It is therefore evident that conventional anti-cancer therapies are not completely effective against lung cancer and new types of drugs need to be developed.

Chemotherapy remains an integral part of lung cancer treatment, usually in combination with surgery and radiotherapy [6]. Cisplatin, a platinum-based metallodrug, is commonly used in clinical practice against a wide range of solid tumours, including lung cancer, especially as part of combination therapy [7,8]. However, the development of resistance to such cisplatin-based chemotherapy is the problem for oncological patients, in addition to negative side effects (e.g.,

* Corresponding author. Department of Pharmacology and Toxicology, Veterinary Research Institute, Hudcova 296/70, Brno, 621 00, Czech Republic.
** Corresponding author. Department of Inorganic Chemistry, Faculty of Science, Palacký University Olomouc, 17. listopadu 12, Olomouc, 77146, Czech Republic.
E-mail addresses: jan.hosek@vri.cz (J. Hošek), pavel.starha@upol.cz (P. Štarha).

https://doi.org/10.1016/j.ejmech.2025.117970
Received 23 May 2025; Received in revised form 10 July 2025; Accepted 11 July 2025
Available online 11 July 2025

nephrotoxicity or myelosuppression).

With the discovery of the antineoplastic effects of cisplatin in 1965, compounds of other d-block metals (including *cis*-[Ru(NH$_3$)$_4$(OH)Cl]Cl; Fig. 1) were also studied for their biological activity [9]. The biological potential of non-platinum complexes, including those of ruthenium (Ru), was further explored [10], and over the years, several Ru complexes have entered clinical trials for the treatment of various types of cancer, including lung cancer, in human cancer patients [11–14]. These achievements make Ru one of the most promising d-block metals in the field of anticancer drug development. Importantly, its success was followed by other group 8 (Os; see Fig. 1 for [Os(η^6-pcym)Cl$_2$(pta)]) [15] and group 9 (Rh, Ir) [15,16] platinum metals offering similar chemistry and structural types; pcym = 1-methyl-4-(propan-2-yl)benzene (*p*-cymene), pta = 1,3,5-triaza-7-phosphaadamantane [14,17].

These metals generally offer various biologically promising structural types, including half-sandwich one [14,17–20]. Half-sandwich complexes consist of a η-coordinated arene (for Ru and Os) or arenyl (for Rh and Ir) ligand, along with three others coordination sites, usually occupied by one bidentate and one monodentate ligand. While the monodentate ligand (e.g., halogenido or pta) can ensure the hydrolytic activation of such complexes, the bidentate ligand is primarily responsible for modulating the biological activity. Furthermore, although not yet fully elucidated, the mechanism of action (MoA) of anticancer half-sandwich Ru, Os, Rh and Ir complexes appears to differ from the conventional anticancer metallodrug cisplatin and its Pt-based analogues [14,18,20]. Their MoA is thought to be multifaceted, involving enhanced production of reactive oxygen species (ROS), interactions with proteins, and disruption of mitochondrial function. Unlike cisplatin, DNA does not appear to be the main target of Ru, Os, Rh, and Ir half-sandwich complexes.

Based on these assumptions, we chose in this work one of the most basic bidentate ligands - ethylene-1,2-diamine (en) - which was used in pioneer papers reporting among the first on anticancer activity of Ru and Os half-sandwich complexes, such as [Ru(η^6-bip)Cl(en)]PF$_6$ (RM175; Fig. 1) and its Os analogue [Os(η^6-bip)Cl(en)]PF$_6$ (AFAP51) [21,22]. We then modified en through a Schiff condensation with DNA-targeting substituents from a family of polycyclic aromatic hydrocarbons (PAHs), namely 2-naphtyl (for L1), 9-anthracenyl (for L2), 9-phenanthrenyl (for L3) or 1-pyrenyl (for L4). We hypothesized that this chemical modification would result in strong intercalative interaction with DNA [23], while the ability of complexes bearing such ligand to generate high ROS populations will be not reduced. Overall, this combined biological effect could lead to high antiproliferative activity and the ability of such rationally designed coordination compounds to overcome acquired resistance of tumour cells.

2. Results and discussion

2.1. Synthesis and general properties

Compounds L1–L4 (Fig. 2 and Supporting Information, Fig. S1) were prepared by a standard Schiff base condensation of en and the appropriate aldehydes of PAHs. Compounds L1, L2, and L4 were formerly reported in the literature [24–27], and their composition and purity were checked by elemental analysis and ^{1}H NMR. Compound L3 is new and is reported here for the first time.

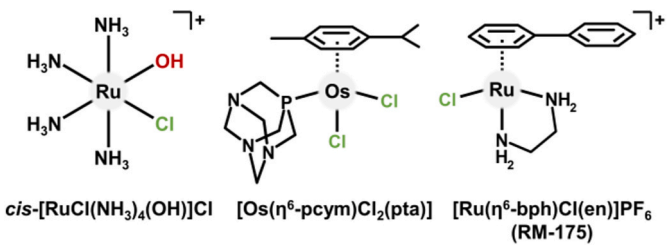

Fig. 1. Pioneer anticancer Ru and Os complexes.

Complexes [Ru(η^6-pcym)Cl(L)]PF$_6$ (**1**–**4**), [Os(η^6-pcym)Cl(L)]PF$_6$ (**5**–**8**), [Rh(η^5-Cp*)Cl(L)]PF$_6$ (**9**–**12**) and [Ir(η^5-Cp*)Cl(L)]PF$_6$ (**13**–**16**) (Fig. 2 and Supporting Information, Fig. S2) were synthesized using microwave-assisted methods, following typical protocols for this type of Ru(II)/Os(II) arene and Rh(III)/Ir(III) arenyl complexes. The starting compounds were the corresponding dimers [M′(μ-Cl)(η^6-pcym)Cl]$_2$ (M′ = Ru or Os) and [M′′(μ-Cl)(η^5-Cp*)Cl]$_2$ (M′ = Rh or Ir). Complex **4** has been previously reported in the literature [28], while other complexes (**1**–**3**, **5**–**16**) are reported here for the first time. Formerly reported complex [Ru(η^6-pcym)Cl(en)]PF$_6$ (**0**) was involved in this study for comparative purposes [21].

The complexes were characterized by CHN elemental analysis, mass spectrometry (MS), nuclear magnetic resonance (NMR), and Fourier Transform Infrared Spectroscopy (FT-IR) (see Experimental section). The formation of the [M′(η^6-pcym)Cl(L)]$^+$ (M′ = Ru for **1**–**4** and Os for **5**–**8**) and [M′′(η^5-Cp*)Cl(L)]$^+$ (M′′ = Rh for **9**–**12** and Ir for **13**–**16**) complex cations was clearly proved by ESI+ MS through the detection of dominant peaks corresponding to the [M′Cl(L)(pcym)]$^+$ and [M′′Cl(Cp*)(L)]$^+$ species, assigned based on their *m/z* values and characteristic isotopic patterns (Supporting Information, Fig. S3–S18); ESI+ refers to electrospray ionization in positive ionization mode. In addition to these pseudomolecular peaks of complex cations of the prepared coordination compounds **1**–**16**, fragment of general compositions {[M′(L)(pcym)]–H}$^+$ and {[M′′(Cp*)(L)]–H}$^+$ were detected in the mass spectra of the studied compounds.

The purity of complexes **1**–**8** was checked by HPLC and the results indicate acceptable purity (96.2–98.4 %) for the following chemical and biological studies (Supporting Information, Fig. S19).

2.2. NMR characterization

The ^{1}H NMR spectra of the free ligands L1–L4 (measured in CDCl$_3$) showed the characteristic –C*H*– Schiff base group resonance as a singlet at 8.46–9.50 ppm (Supporting Information, Fig. S20–S23). This resonance was accompanied by a complex aromatic region with numerous multiplets in the 7.12–8.92 ppm range assignable to the PAH substituents, and by a singlet belonging to aliphatic ethylene protons (4.08–4.52 ppm). In the case of L2, residual signals of free anthracene-9-carbaldehyde (e.g., 11.53 ppm for –C*H*O) were detected in CDCl$_3$, even after purification by several recrystallizations. The same behaviour was observed in DMSO-d_6, whereas in deuterated benzene (C$_6$D$_6$), only the signals of L2 were detected. This implied that L2 is partially unstable in CDCl$_3$ and DMSO-d_6, but it can be used for the preparation of complexes, since it was prepared in adequate purity, as proved by ^{1}H NMR in C$_6$D$_6$ (Supporting Information, Fig. S21).

The discussion of the NMR results is divided into two parts. First, Ru and Os complexes **1**–**8** will be discussed. Their ^{1}H NMR spectra were measured in DMSO-d_6 and contained all the expected resonances with appropriate integral intensities (Supporting Information, Fig. S24–S27). The singlet corresponding to the –C*H*– Schiff base group was detected at lower fields (9.37–10.24 ppm) as compared with free ligands. Importantly, no changes were observed for this characteristic resonance (0–24 h), demonstrating that no cleavage of the used en-based ligands L1–L4 occurred and that the Ru and Os complexes **1**–**8** are stable in the used solvent (DMSO-d_6). As a consequence of the coordination of L1–L4 to the metal centres, the ethylene hydrogens showed as two broad signals at 3.63–4.45 ppm in the spectra of **1**–**8**. The presence of pcym was proved by its characteristic set of resonances, for example by two doublets (or broad signals) at 4.05–5.79 ppm (aromatic hydrogens of pcym), or by a singlet at 1.60–2.39 ppm (methyl of pcym).

In contrast to Ru and Os complexes **1**–**8**, their Rh and Ir analogues **9**–**16** were unstable in the used solvents (CDCl$_3$, DMSO-d_6). Specifically, gradual cleavage of the Schiff base bond was observed, resulting in the release of the PAH substituents, as proved by detection of the signals of

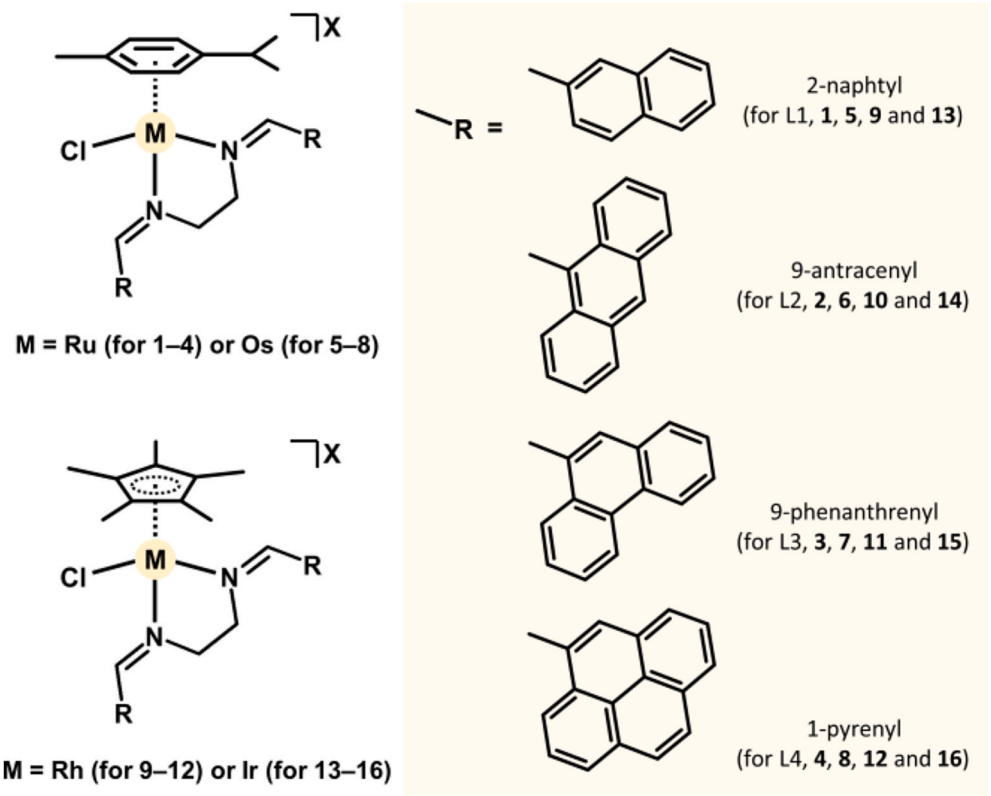

Fig. 2. General structural formulas of the studied complexes **1**–**16**, given together with their polycyclic aromatic substituents.

free PAH carbaldehydes, while the characteristic singlet of the –C*H*– Schiff base group gradually disappeared in ^{1}H NMR spectra of Rh and Ir complexes **9**–**16** (Supporting Information, Fig. S28–S31). Only the L1-containing complexes **9** and **13** were stable enough to obtain their ^{1}H NMR spectrum before the beginning of degradation (Supporting Information, Fig. S28), but their hydrolytic stability was poor (see below). The spectra of other Rh and Ir complexes (**10**–**12** and **14**–**16**) contained the resonances of the degradation products (e.g. singlets of carbaldehydes or more Cp* resonances) even in the very fresh solutions (t > 5 min; Supporting Information, Fig. S29–S31).

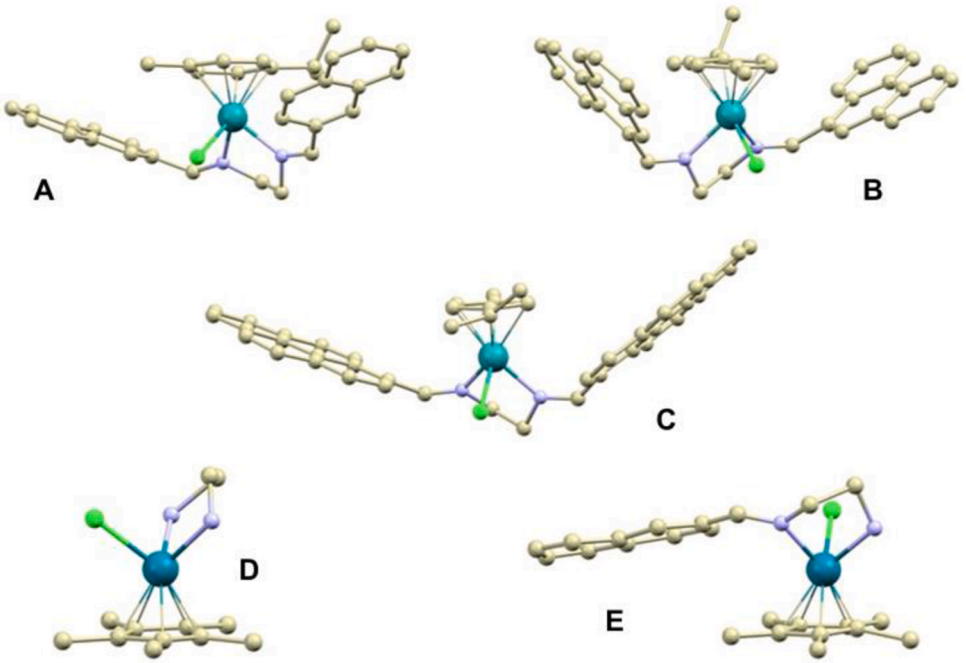

Fig. 3. The molecular structures of the complex cations in compounds **1** (**A**), **3** (**B**) and **4** (**C**), and in fragments **9'** (**D**) and **13'** (**E**). The PF_6^- anions and hydrogen atoms were omitted for clarity. The colour code used is as follows: light yellow (carbon), green (chlorine), dark teal (metal atom) and light blue (nitrogen). (For interpretation of the references to colour in this figure legend, the reader is referred to the Web version of this article.)

Given the pronounced instability of Rh and Ir complexes **9**–**16**, they were excluded from the following chemical analysis (CHN analysis, FTIR spectroscopy), as well as from the stability studies in the presence of water and biological assays.

2.3. Crystal structures

We successfully prepared single crystals of Ru compounds **1**, **3** and **4**, which were suitable for single-crystal X-ray diffraction (Supporting Information, Tables S1 and S2). The experiments confirmed the anticipated composition of these compounds, revealing complex cations paired with PF_6^- anions. The complex cations consist of arene ligand, one bidentate Schiff base, and one chlorido ligand within the inner coordination sphere, forming a pseudo-octahedral piano-stool arrangement (Fig. 3A–C). The longest metal-ligand bond lengths observed are the Ru−Cl bonds, which measure approximately 2.40 Å in all three complexes. In contrast, the Ru−N bonds are shorter and more variable, ranging between 2.09 and 2.13 Å. All metal–ligand bond lengths are summarized in Supporting Information, Table S3.

During the crystallization of compounds **9** and **13**, we isolated crystals that contained partially (for **9**) or fully (for **13**) cleaved Schiff base ligands. In the Rh complex **9**, the Schiff base ligand in the resulting structure of [Rh(η^5-Cp*)Cl(en)]PF_6 (**9′**) was fully cleaved with both the naphthyl moieties released and leaving ethylene-1,2-diamine (en) to act as the N,N′-chelating ligand (Fig. 3D). Regarding the Ir complex **13**, the resulting structure [Ir(η^5-Cp*)Cl(L1′)]PF_6 (**13′**) contains a partially cleaved Schiff base ligand *N*-(naphthalen-2-ylmethylidene)ethane-1,2-diamine with only one 2-naphtyl substituent (L1′; Fig. 3E). Both complexes **9′** and **13′** adopt a pseudo-octahedral piano-stool arrangement, similar to those observed in compounds **1**, **3** and **4**. The [Rh(η^5-Cp*)Cl(en)]$^+$ cation of **9′** was formerly reported in the literature [29].

2.4. Aqueous chemistry

Ru and Os complexes **1**–**8** and 2-naphthyl-bearing compounds **9** (Rh) and **13** (Ir), which showed acceptable stability in $CDCl_3$ and DMSO-d_6 (see above), were investigated by ^{1}H NMR for their stability in a water-containing mixture of solvents (50 % DMSO-d_6/50 % D_2O with PBS); PBS = phosphate-buffered saline (pH 7.4), added to mimic physiological conditions (pH, chloride ions).

Regarding Rh and Ir complexes **9** and **13**, the results revealed that both the complexes underwent rapid degradation associated with a release of the PAH substituent (Fig. 4 and Supporting Information, Fig. S32 and S33). The characteristic resonances of free 2-naphthaldehyde were detected (e.g., the –C*H*O resonance at 9.99 ppm). The initial complexes were transformed in 5 h (for **9**) and in 20 h (for **13**). After these times, two sets of resonances were detected in the spectra instead of the initial Schiff bond resinance. One was clearly assignable to the released 2-naphthaldehyde (δ = 9.99 ppm for both **9** and **13**), while the second one (δ = 8.98 ppm for **9** and 9.10 ppm for **13**) most likely corresponded to fragments [M(η^5-Cp*)Cl(L1′)]$^+$ (**9′**, **13′**) with only one 2-naphthaldehyde substituent (L1′). Similar fragmentation was detected by a single-crystal X-ray analysis of **13'** (see above; Fig. 3).

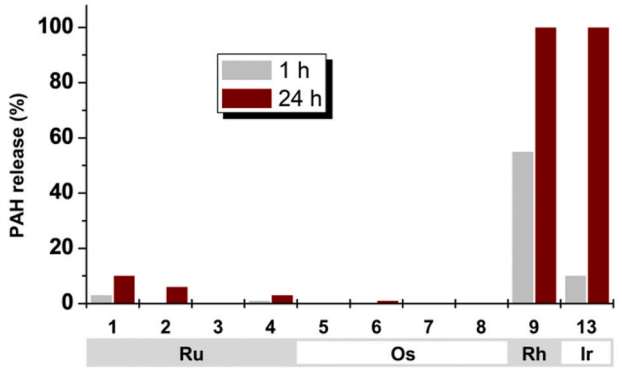

Fig. 4. Extent of the release of polycyclic aromatic substituents (PAHs) from the studied complexes, as determined by ^{1}H NMR in 50 % DMSO-d_6/50 % D_2O with phosphate-buffered saline (PBS, pH 7.4). An extent of the PAH release was calculated from an integral intensity of the –C*H*– Schiff bond resonance (i.e. bound PAH substituent in complexes) and the –C*H*O resonance of a free carbaldehyde (i.e. released PAH substituent).

Analogical 2-naphthyl-bearing Ru (**1**) and Os (**5**) complexes were markedly more stable than their Rh (**9**) and Ir (**13**) congeners. Complex **1** released less than 1 % of its PAH substituent in 50 % DMSO-d_6/50 % D_2O with PBS after 1 h of standing at r.t. (Fig. 4 and Supporting Information, Fig. S34). A similar extent of PAH release was observed by ^{1}H NMR in the presence of excess of NADH coenzyme (5 molar equiv.), which was used as a model highly-concentrated intracellular biomolecule (Supporting Information, Fig. S34). For this mixture of **1** with NADH, only negligible NADH oxidation (ca. 4 % of NADH) was detected by ^{1}H NMR. In contrast with **9** and **13**, no new set of signals assignable to the fragments with only one 2-naphthaldehyde substituent (L1′) was found in the ^{1}H NMR spectra of **1** or its mixture with excess NADH. Os complex **5** was the most stable of the L1-bearing complexes **1**, **5**, **9** and **13**, because **5** did not undergo any changes when dissolved alone or in a mixture with excess NADH (5 molar equiv.) for 24 h (50 % DMSO-d_6/50 % D_2O with PBS; Fig. 4 and Supporting Information, Fig. S35). Only negligible NADH oxidation (ca. 2 % of NADH) was observed for the mixture of **5** with an excess of NADH, which was not accompanied by the release of the 2-naphthaldehyde substituent of **5**.

Similarly to the L1-containing complexes **1** and **5**, their analogues **2**–**4** and **6**–**8** with more extended PAH substituent (in L2–L4) were found to be adequately stable in the used DMSO/D_2O mixture of solvents after 1 h of standing at r.t. (Fig. 4). This finding of sufficient stability allowed subsequent biological experiments to be performed on compounds **1**–**8**. In contrast, complexes **9**–**16** were not suitable for the planned biological experiments due to low stability in DMSO (section 2.2) or its mixture with water (this section).

2.5. In vitro cytotoxicity on 2D and 3D cell models

To evaluate the therapeutic potential against lung cancer, a screening cytotoxicity assay was conducted on several cell lines. In addition to lung cancer-derived cell lines (the epithelial cell line A549, the adenocarcinoma cell line MOR, and its cisplatin-resistant variant MOR/CPR), the assay also included the foetal lung tissue cell line MRC-5 and human peripheral blood mononuclear cells (PBMCs) (Table 1).

Generally, Os(II) complexes **5**–**8** showed higher cytotoxic effect than their Ru(II) analogues **1**–**4**, as it was previously demonstrated on other complexes and cell lines (e.g., Refs. [30–32]). The most cytotoxic was Os (II) complex **5**, which showed the highest potential across all cell lines. This compound together with its Ru(II) analogue **1** were selected for further analysis to reveal mechanisms of action.

It is worth noting that all tested complexes were more active against cisplatin-resistance MOR/CPR cell line than against cisplatin-sensitive MOR. This indicates the ability of these molecules to bypass several drug resistances. All complexes were also more cytotoxic than cisplatin against all used cell lines. On the other hand, no selectivity towards cancerous cell lines was observed.

A previous investigation reported on biological and catalytic activity of similar Ru compounds derived from two different en-based Schiff bases, including complex **4** with L4 (the second one is N,N′-bis{(*E*)-[4-(L-methylethyl)phenyl]methylene}ethane-1,2-diamine (L5)) [28]. Both compounds were tested for *in vitro* antitumor activity against human breast adenocarcinoma (MCF7) and human hepatocellular carcinoma (HepG2) cell lines. The compound [Ru(η^6-pcym)Cl(L5)]PF_6 showed only low *in vitro* cytotoxicity on these human cell lines (IC_{50} = 74.9 and 115.5 μM, respectively), whereas **4** was inactive on the human cell lines used in the concentration range tested (IC_{50} > 200 μM). However, it is

Table 1
The results (IC_{50}; given as mean ± SE and 95 % confidence interval [μM]) of *in vitro* testing of antiproliferative activity of compounds **1**–**8** against human lung carcinomas (A549, MOR), human cisplatin-resistant lung carcinoma (MOR/CPR), human foetal lung fibroblasts (MRC-5), and human peripheral blood mononuclear cells (PBMCs); CCK-8 assay, 72 h exposure time. Cisplatin (CDDP) and complex [Ru(η^6-pcym)Cl(en)]PF_6 (**0**) were used as the reference drugs.

Compd.	Cell line				
	A549	MOR	MOR/CPR	PBMCs	MRC-5
1	6.0 ± 1.1 (4.7–7.8)	3.1 ± 1.2 (2.2–4.6)	2.1 ± 1.1 (1.6–2.7)	1.7 ± 1.1 (1.5–2.0)	6.2 ± 1.1 (5.5–7.2)
2	3.3 ± 1.2 (2.3–4.8)	4.2 ± 1.0 (3.9–4.5)	3.0 ± 1.1 (2.5–3.6)	1.1 ± 1.1 (1.0–1.3)	1.4 ± 1.2 (0.9–2.0)
3	3.9 ± 1.1 (3.1–4.9)	5.1 ± 1.1 (4.2–6.3)	2.0 ± 1.0 (1.9–2.2)	1.1 ± 1.2 (0.8–1.6)	1.9 ± 1.1 (1.7–2.2)
4	3.0 ± 1.2 (2.1–4.1)	3.6 ± 1.1 (2.9–4.8)	2.6 ± 1.1 (2.2–3.0)	0.5 ± 1.1 (0.4–0.6)	0.7 ± 1.2 (0.5–1.3)
5	1.2 ± 1.2 (0.9–1.6)	1.7 ± 1.1 (1.3–2.1)	0.5 ± 1.1 (0.4–0.6)	0.6 ± 1.0 (0.5–0.7)	1.6 ± 1.1 (1.4–1.8)
6	3.4 ± 1.1 (2.5–4.4)	5.2 ± 1.0 (4.7–5.7)	2.9 ± 1.0 (2.7–3.1)	0.2 ± 1.2 (0.1–0.3)	2.8 ± 1.1 (2.4–3.9)
7	1.5 ± 1.2 (1.1–2.2)	2.8 ± 1.1 (2.4–3.2)	2.0 ± 1.1 (1.7–2.8)	1.3 ± 1.2 (1.0–1.8)	0.8 ± 1.0 (0.7–0.9)
8	2.2 ± 1.2 (1.5–3.2)	3.8 ± 1.1 (3.2–5.1)	2.2 ± 1.1 (1.6–2.9)	0.5 ± 1.2 (0.3–0.6)	0.8 ± 1.0 (0.7–0.8)
0	>10	>10	Not tested	Not tested	Not tested
CDDP	10.4 ± 1.1 (8.6–12.4)	6.3 ± 1.1 (5.4–7.6)	>20	8.6 ± 1.0 (7.7–9.5)	2.6 ± 1.1 (2.3–3.0)

worth noting that in this experiment only 24 h incubation was used (in the comparison with 72 h used in our study). Complex [Ru(η^6-pcym)Cl(en)]PF_6 (**0**), which was formerly reported to be cytotoxic in various human cancer cell lines (e.g. A2780 ovarian carcinoma) [28], was involved in this study for comparative purposes. **0** did not show any cytotoxicity in A549 and MOR cells (Table 1), which indicates that the presence of PAH substituents in highly cytotoxic compounds **1**–**8** is responsible for the cytotoxic effect.

Based on obtained results, complex **5**, as the most potent compound, and its ruthenium analogue **1** were selected to further *in vitro* analyses. To verify the anticancer potential of selected complexes **1** and **5**, their effect on 3D cell culture model was analyzed. This model is closer to real tumour and fill the gap between common 2D cell cultures and animal *in vivo* experiments. The ability of complexes **1** and **5** to cause cell death in 3D spheroids formed from A549 cell was analyzed (Fig. 5 and Supporting Information, Fig. S36). Obtained results demonstrated similar potential of tested complexes to induce cell death as cisplatin (CDDP).

2.6. Cell cycle and apoptosis evaluation

Modification of cell cycle and induction of apoptosis is a common mechanism of action of cytostatics. Tested complexes **1** and **5** did not significantly affect cell cycle (Fig. 6). Only minor non-significant G1 arrest was visible after treatment with these compounds, apart from cisplatin, which caused significant G2/M arrest. Several studies demonstrated that the ability of Ru(II) and Os(II) complexes to affect cell cycle strongly depends on type of ligand and cell line. However, it is possible to summarize that most of studied Ru and Os complexes tend to cause G1/G0 arrest [33,34].

On the other hand, it can be supposed that **1** and **5** were able to induce apoptosis after 24 h incubation and this effect was dissipated after prolonged (72 h) incubation (Fig. 6). The ability to induce apoptosis has been described for many Ru(II) and Os(II) complexes, but there is not clear structure-activity relationship [34,35]. The level of apoptotic cells was relatively low after 24 h incubation – 11.9 % for CDDP, 16.6 % for **1**, and 12.8 % for **5**, when high concentration of both tested complexes was used (3 × IC_{50}). The number of necrotic cells was low, as well – 0.8–1.4 % after 24 h and 1.7–2.2 % after 72 h. The only exception was CDDP which caused necrosis in 11 % of cell after 72 h incubation. These results indicate that tested complexes **1** and **5** trigger different type of cell death than apoptosis or necrosis.

2.7. Mitochondrial membrane potential and mitochondria visualisation

Although only low induction of apoptosis was observed in cells after incubation with complexes **1** and **5**, the change of mitochondrial membrane potential ($\Delta\psi_m$) was evaluated as it could be connected with early stages of apoptosis [36].

Complex **5**, as well as cisplatin, was able to significantly disrupt the $\Delta\psi_m$ after 24 h incubation with 7.1 % and 7.4 % of cells with depolarised mitochondrial membrane, respectively, whereas complex **1** had only minor effect (2.3 % of cells with depolarised mitochondrial membrane) (Fig. 7A). This effect was eliminated after prolonged (72 h) incubation with tested compounds (Supporting Information, Fig. S37). Our results indicate a greater effect of Os(II) complex **5** on mitochondrial function than Ru(II) compound **1**, as earlier reported for different pair of Ru and Os complexes [32].

It is in the accordance with previous studies, where similar half-sandwich Ru(II) complexes have demonstrated a remarkable ability to depolarize mitochondrial membranes. For instance, a specific Ru(II) complex exhibited an eightfold increase in mitochondrial depolarization in A549 lung cancer cells within just 1 h treatment. This rapid depolarization indicates a potent mechanism by which these complexes induce mitochondrial dysfunction [37].

Further studies have shown that Ru(II) complexes can induce apoptosis through mitochondrial pathways. The Ru(II) complex HB324, for example, activates the pro-apoptotic protein Harakiri, which inhibits anti-apoptotic proteins Bcl-2 and BCL-xL, leading to mitochondrial outer membrane permeabilization and subsequent cell death [38]. Additionally, half-sandwich Ru(II) complexes have been observed to impair mitochondrial function by reducing both mitochondrial membrane potential and respiration, further contributing to their cytotoxic effects on cancer cells [39].

The effect of Os(II) complexes is less described, but several studies have confirmed their role in $\Delta\psi_m$ disruption. For instance, Os(II) arene complexes with azopyridine ligands have demonstrated potent anticancer activity in A549 human non-small cell lung cancer cells, caused, at least, by the change of $\Delta\psi_m$ [40].

Tested complexes **1** and **5** were also able to increase the mitochondrial mass in cells (Fig. 7B and C). This behaviour could be understood as compensation mechanisms of disrupted mitochondrial functions. According to our best knowledge, this effect was observed for Ru(II) and Os (II) complexes for the first time. However, high content of mitochondria in cells has related to cisplatin resistance [41]. On the other hand, high mitochondria mass increased sensitivity to pemetrexed treatment [41] and elevated production of ROS, contributing to oxidative stress and enhancing the cytotoxic effects of the drug [42].

2.8. Stress-related gene expression

To reveal the potential mode of action of tested complexes, their effect on expression of stress-related genes was evaluated. The effect of complexes **1** and **5** was described on cancerous (A549; Fig. 8) and non-cancerous (differentiated HepaRG; Fig. 9) cells, which mimic the primary hepatocytes responsible for elimination of xenobiotics from a body.

In most cases, Ru(II) complex **1** affected gene expression more effectively than its Os(II) analogue **5** in A549 cells. Both the studied complexes appear to target cellular organelles and proteins, eliciting multi-faceted stress responses.

Consistent with possible proteotoxic and organelle stress, complexes **1** and **5** strongly engage the unfolded protein response (UPR)/endoplasmic reticulum (ER) stress, both in A549 and HepaRG cells. On the other hand, DDIT3 expression was not affected in HepaRG cells treated by cisplatin. Complexes **1** and **5** upregulate DDIT3 (aka CHOP), a

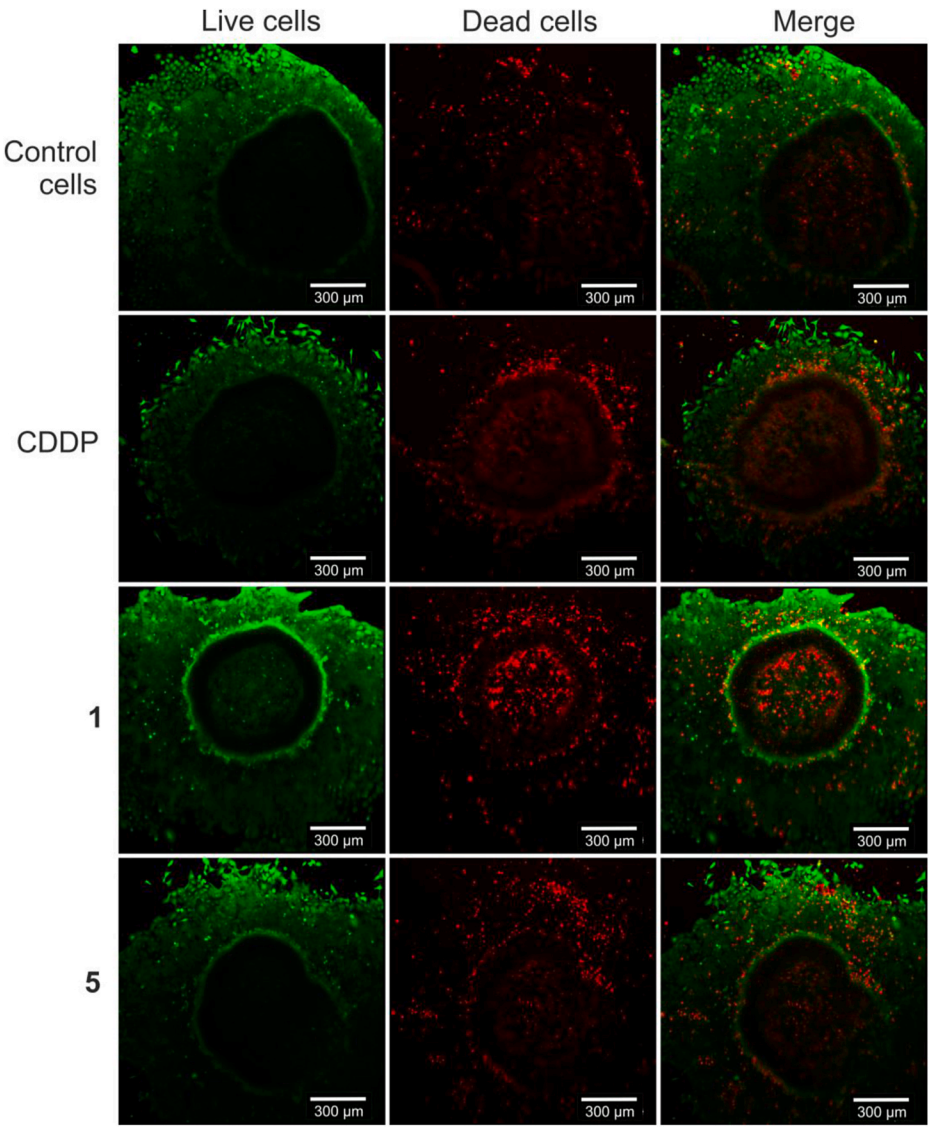

Fig. 5. 3D spheroids from A549 cells were treated with complex **1** and **5** and cisplatin (CDDP) at concentrations corresponding to the IC_{50} values obtained from 2D experiments (i.e., 6 μM for **1**, 1.2 μM for **5**, and 10 μM for cisplatin). After 72 h of incubation, the spheroids were stained with a Live/Dead Cell Imaging Kit to distinguish live (green) and dead (red) cells, and confocal microscopy was used to capture the images (magnification 10 ×). Cisplatin (CDDP) was used as the reference drug. (For interpretation of the references to colour in this figure legend, the reader is referred to the Web version of this article.)

sentinel of unresolved ER stress-induced apoptosis, and ATF3, an adaptive stress-response transcription factor, in a concentration-depended manner. A striking finding is that **1** and **5** treatment down-regulates HSPA5 (BiP/GRP78), the master ER chaperone. HSPA5 normally helps refold misfolded proteins and suppress UPR sensor gene activation; its suppression by HSPA5 depletion would amplify ER stress signalling. In cells exposed to complexes **1** and **5**, GDF15 is indeed upregulated alongside DDIT3 and ATF3, reinforcing the notion that these compounds elicit an ER stress response akin to HSPA5 inhibition. The outcome of severe UPR activation is apoptotic commitment, as DDIT3 drives pro-apoptotic genes and inhibits Bcl-2 family survival proteins. In line with this, global transcriptomic analyses have shown that a structurally different Ru(II) compound (an octahedral polypyridyl complex) preferentially activates ER stress genes compared to cisplatin [43]. In other words, this seems to be the first report on half-sandwich Ru(II) and Os(II) complexes aiming, at least partially, their anticancer activity to ER.

Tested complexes **1** and **5** also activate DNA damage signalling, although to a lesser extent than cisplatin. Treated cells show increased p21 and GADD45A, indicating that some DNA damage or replication stress occurs. This could engage p53 – indeed many Ru-based complexes can activate p53 pathways, though often less potently than cisplatin [43]. In prior comparative analyses, a Ru(II) organometallic compound RDC11 induced p53-dependent genes to a lesser degree than cisplatin, which aligns with a more moderate DNA damage profile. Instead, RDC11 favoured other stress responses (oxidative and ER stress) over the classical p53 response [43]. Thus, complexes **1** and **5** likely trigger p53 and cell-cycle arrest as a secondary consequence of DNA damage, while their primary cytotoxic signals come from proteotoxic and metabolic stress. Apart from cisplatin that induces a broader and more intense set of DNA damage response genes than formerly reported Ru(II) and Os(II) complexes. In this context, adding a 2-naphtyl PAH substituent to the structures of **1** and **5** was hypothesized to increase their ability to intercalate DNA, as reported for similar Ru(II) complexes derived from polycyclic aromatic diamines, which showed a dramatic increase of DNA intercalation and binding [44]. Thus **1** and **5** may partially act by wedging into DNA and inducing damage or transcriptional dysregulation. However, unlike cisplatin, they are not expected to primarily create fixed crosslinks; instead, they might form monofunctional adducts or associate with DNA transiently, evoking different DNA damage

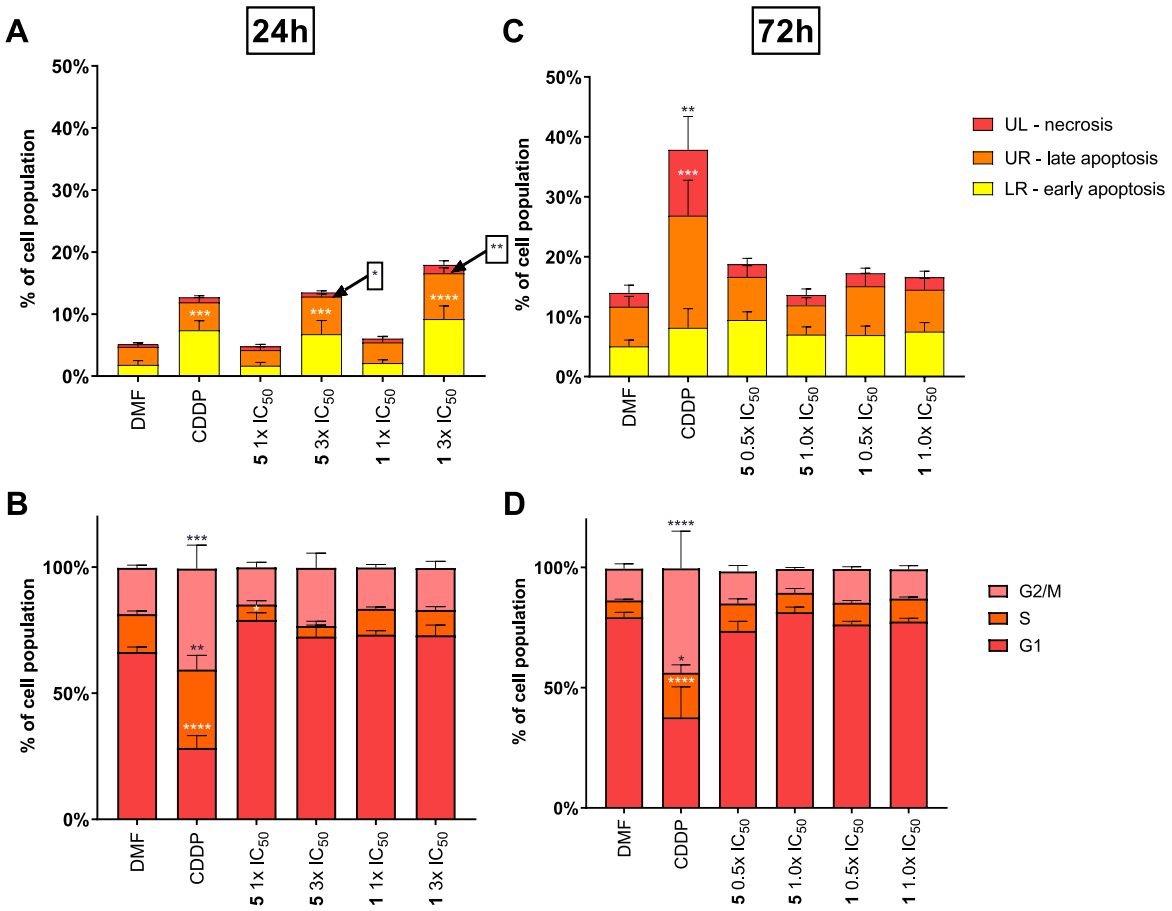

Fig. 6. The effect of **1** and **5** on cell death (**A**, **C**) and on the cell cycle (**B**, **D**) detected in the A549 cell line. The cells were incubated with the test compounds at the IC_{50}, half-IC_{50}, and triple-IC_{50} concentrations (i.e., 3.0, 6.0, and 18.0 μM for **1**; 0.6, 1.2, and 3.6 μM for **5**). Cisplatin (CDDP) at a concentration of 10 μM served as the positive control. The analysis was performed after 24 h (**A**, **B**) and 72 h (**C**, **D**) of exposure. The data are shown as the mean ± SEM; * indicates statistical significance ($p < 0.05$) compared with the DMF group; ** indicates statistical significance ($p < 0.01$) compared with the DMF group; *** indicates statistical significance ($p < 0.001$) compared with the DMF group; **** indicates statistical significance ($p < 0.0001$) compared with the DMF group. The quadrants of the dot plots for cell apoptosis/death were as follows: early apoptosis, lower right quadrant (LR); late apoptosis, upper right quadrant (UR); and necrotic/dead cells, upper left quadrant (UL).

signalling dynamics.

Importantly, complexes **1** and **5** do not significantly induce IL-6 or IL-8 in cancerous A549 cells, unlike cisplatin, that robustly induces IL-6 and IL-8 transcripts (and protein secretion) as part of an acute response (Fig. 8) [45]. The gene expression data show no upregulation of these inflammatory cytokines with **1** and **5** treatment. This suggests minimal activation of NF-κB or senescence-associated secretory programs by **1** and **5**. The absence of an IL-6/8 response could reflect a lack of robust DNA damage-associated pattern recognition (e.g. no cytosolic DNA to trigger innate immune sensors) or a more direct apoptotic elimination of cells before they mount an inflammatory response. In pharmacological terms, this is potentially beneficial – inducing cancer cell death without stimulating pro-inflammatory cytokines might reduce pro-tumour inflammation or paracrine survival loops that cytokines like IL-6 can provide. It underscores a mechanistic difference: cisplatin's damage response crosses into immune signalling, whereas **1** and **5** caused stress response is more contained to the tumour cell's internal stress pathways. On the other hand, the situation is opposite in non-cancerous HepaRG cells - **1** and **5** induced IL-6/8 expression, whereas cisplatin not. The absence of IL-6/8 might also suggest that complexes **1** and **5** do not drive cells into a senescent state but rather push them directly to apoptosis.

Uniquely, complexes **1** and **5** upregulate CYP1A1 in A549 cells, but not in HepaRG cells, a cytochrome P450 enzyme not appreciably induced by cisplatin. On the other hand, in HepaRG cells, the CYP3A4 gene expression was elevated (this gene is not present in A549 cells [46]. CYP1A1 is a classic target of the aryl hydrocarbon receptor (AhR), a ligand-activated transcription factor that senses polyaromatic xenobiotics. The naphthyl-containing ligand in **1** and **5** is a polyaromatic structure that may act as an AhR ligand or be metabolized into one. Induction of CYP1A1 strongly suggests AhR activation, as AhR binding leads to transcription of CYP1A1 as part of the detoxification response [47]. Thus, the cell may recognize **1** and **5** as a xenobiotic stress, engaging chemical detox pathways. Cisplatin, being an inorganic complex without an aromatic moiety, does not trigger this pathway. This difference highlights the pharmacological role of the naphthyl ligand: it essentially flags **1** and **5** as an AhR-active xenobiotic, adding another layer to its mechanism (one that cisplatin lacks).

The oxidative stress indicated as elevated expression of HMOX1 and HSP70 genes was observed only in HepaRG cells treated by Os(II) complex **5**. However, minute elevation of HMOX1 was also observed for Ru(II) complex **1** in A549 cells.

Overall, the gene expression signature for complexes **1** and **5** points to ER stress-mediated apoptosis as a central mechanism, whereas for cisplatin the UPR is more of a secondary, downstream consequence. From a molecular pharmacology standpoint, these differences could

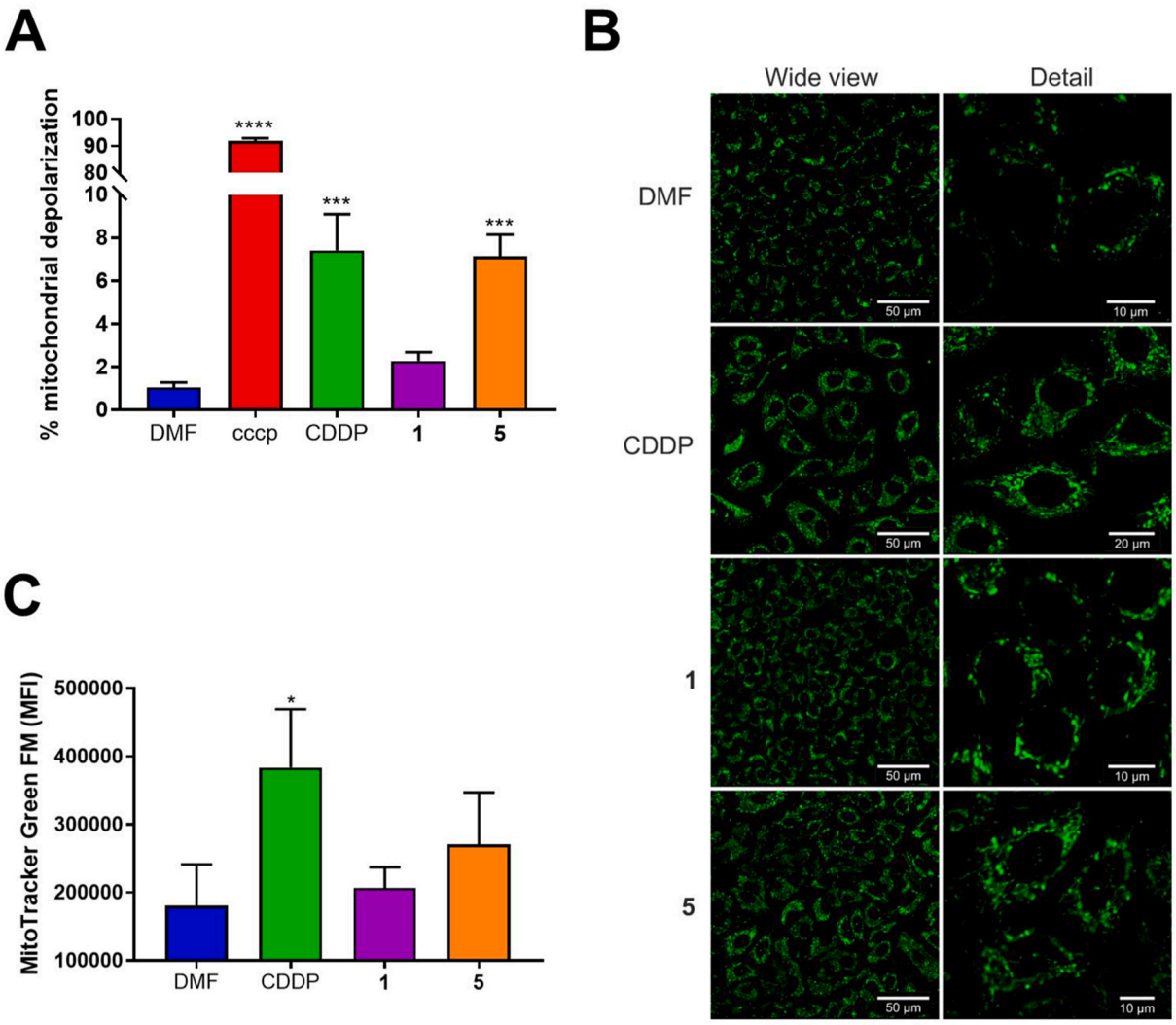

Fig. 7. The effect of **1** and **5** on mitochondrial membrane depolarization in the A549 cell line (**A**). The cells were incubated with the test compounds at the IC_{50} concentrations (i.e., 6 μM for **1** and 1.2 μM for **5**). Cisplatin (CDDP) at a concentration of 10 μM and carbonyl cyanide chlorophenylhydrazone (cccp; 50 μM) were used as a control for impaired mitochondrial membrane potential. The analysis was performed after 24 h of exposure by TMRM staining and confocal microscopy. The effect of **1** and **5** on mitochondrial cellular mass in A549 cells (**B** – **C**). After 72 h incubation of cells with the test compounds at the IC_{50} concentrations and cisplatin (CDDP) at a concentration of 10 μM, they were stained by MitoTracker and observed either under confocal microscopy (magnification 63 × for wide view, digital zoom for detail) (**B**) or by flow cytometry (**C**). The data are shown as the mean ± SEM; * indicates statistical significance ($p < 0.05$) compared with the DMF group; *** indicates statistical significance ($p < 0.001$) compared with the DMF group; **** indicates statistical significance ($p < 0.0001$) compared with the DMF group.

translate to distinct anticancer profiles, including e.g. efficacy in tumours with dysfunctional p53 or resistance towards conventional anticancer drugs (such as cisplatin), since they kill via alternate stresses.

2.9. *In vivo* outlook

Based on their physicochemical stability and potent *in vitro* profile, tested Ru(II) and Os(II) PAH-Schiff base complexes hold considerable therapeutic promise. Their ability to overcome cisplatin resistance *in vitro* by engaging alternative cytotoxic pathways (ER stress and proteotoxic) could translate into efficacy in tumours that are refractory to conventional platinum therapy. Importantly, the minimal pro-inflammatory cytokine response in tumour cells suggests they might provoke less collateral tissue inflammation or immunosuppressive side-effects *in vivo*, potentially improving tolerability. In preclinical animal models, we would expect these complexes to induce robust apoptosis within tumours through mitochondrial/ER stress mechanisms, leading to tumour regressions even in cases with p53 dysfunction or platinum resistance. Toxicity-wise, the available data hint at a favourable profile but warrant careful evaluation: the lack of significant myelosuppression or nephrotoxicity in analogous Ru(III) trials (e.g. KP1339) is encouraging [11] and the new Ru(II) complexes may similarly spare these systems. However, their recognition by AhR and induction of liver enzymes *in vitro* suggest that hepatic metabolism and potential hepatotoxicity will be key considerations. The induction of CYP3A4 in hepatocytes (as seen with Os(II) analogues) and inflammatory cytokines in normal cells indicates that normal tissues might mount a detoxification or stress response to these agents. Thus, while anticancer efficacy may be high, a careful balance between tumoricidal action and host toxicity must be managed. Overall, the PAH-bearing Ru(II) half-sandwich complexes emerge as promising anticancer candidates that could complement or surpass existing Ru(III) drugs. They appear capable of bypassing classic resistance mechanisms and killing cancer cells via nontraditional routes (ER stress and metabolic collapse) while potentially reducing certain side effects. Continued *in vivo* studies and early-phase trials will be crucial to confirm their therapeutic potential,

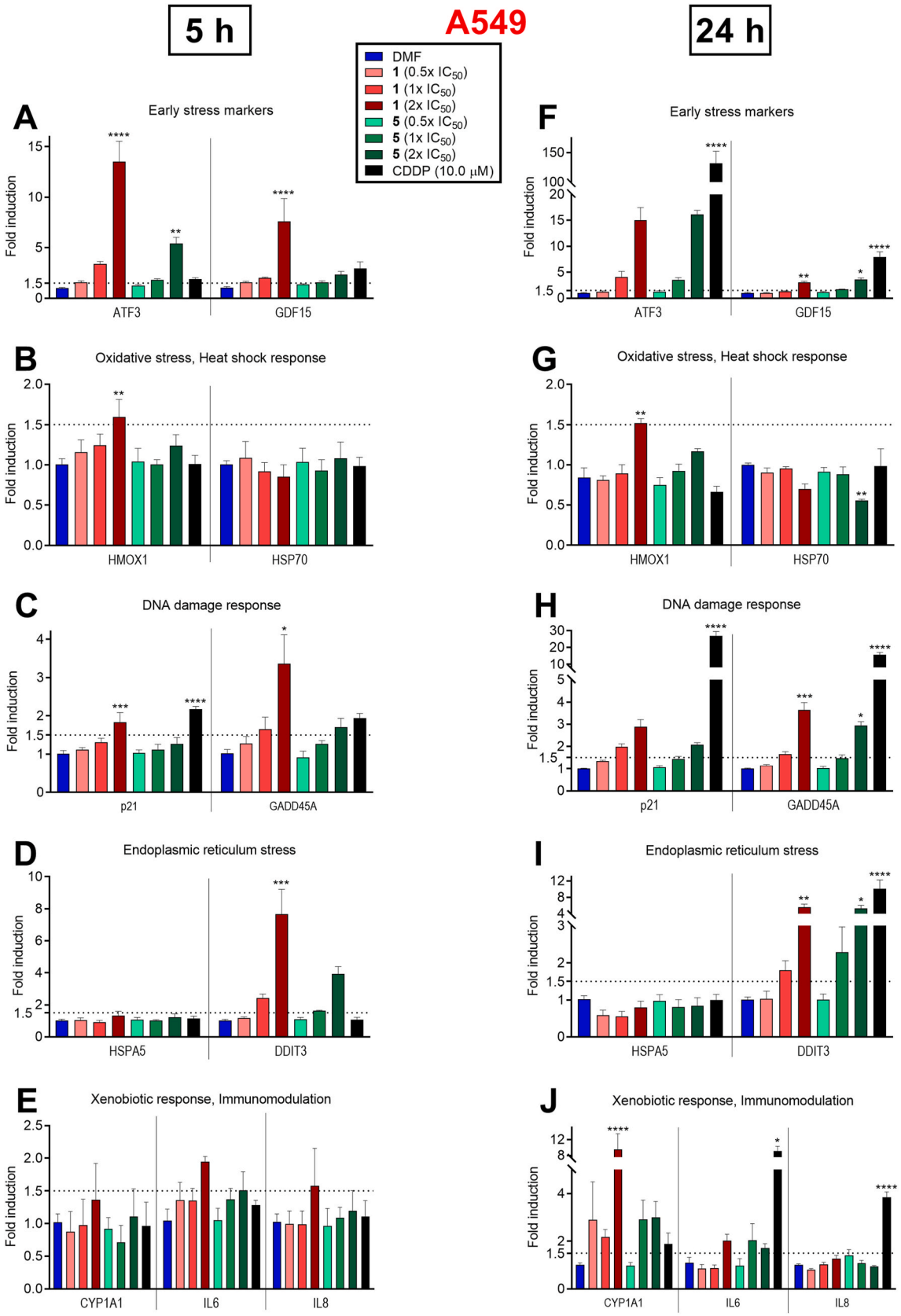

Fig. 8. Changes in the gene expression caused by complexes **1** and **5**, and cisplatin (CDDP) in A549 cancer cells. A549 cells were incubated with tested compounds at the IC_{50}, half-IC_{50}, and double-IC_{50} concentrations (i.e., 3.0, 6.0, and 12.0 μM for **1**; 0.6, 1.2, and 2.4 μM for **5**) or DMF (0.1 % v/v) only for 5 (**A**–**E**) and 24 h (**F**–**J**). The gene expression was evaluated by q-RT-PCR. The data are shown as the mean ± SEM; * indicates statistical significance ($p < 0.05$) compared with the DMF group; ** indicates statistical significance ($p < 0.01$) compared with the DMF group; *** indicates statistical significance ($p < 0.001$) compared with the DMF group; **** indicates statistical significance ($p < 0.0001$) compared with the DMF group.

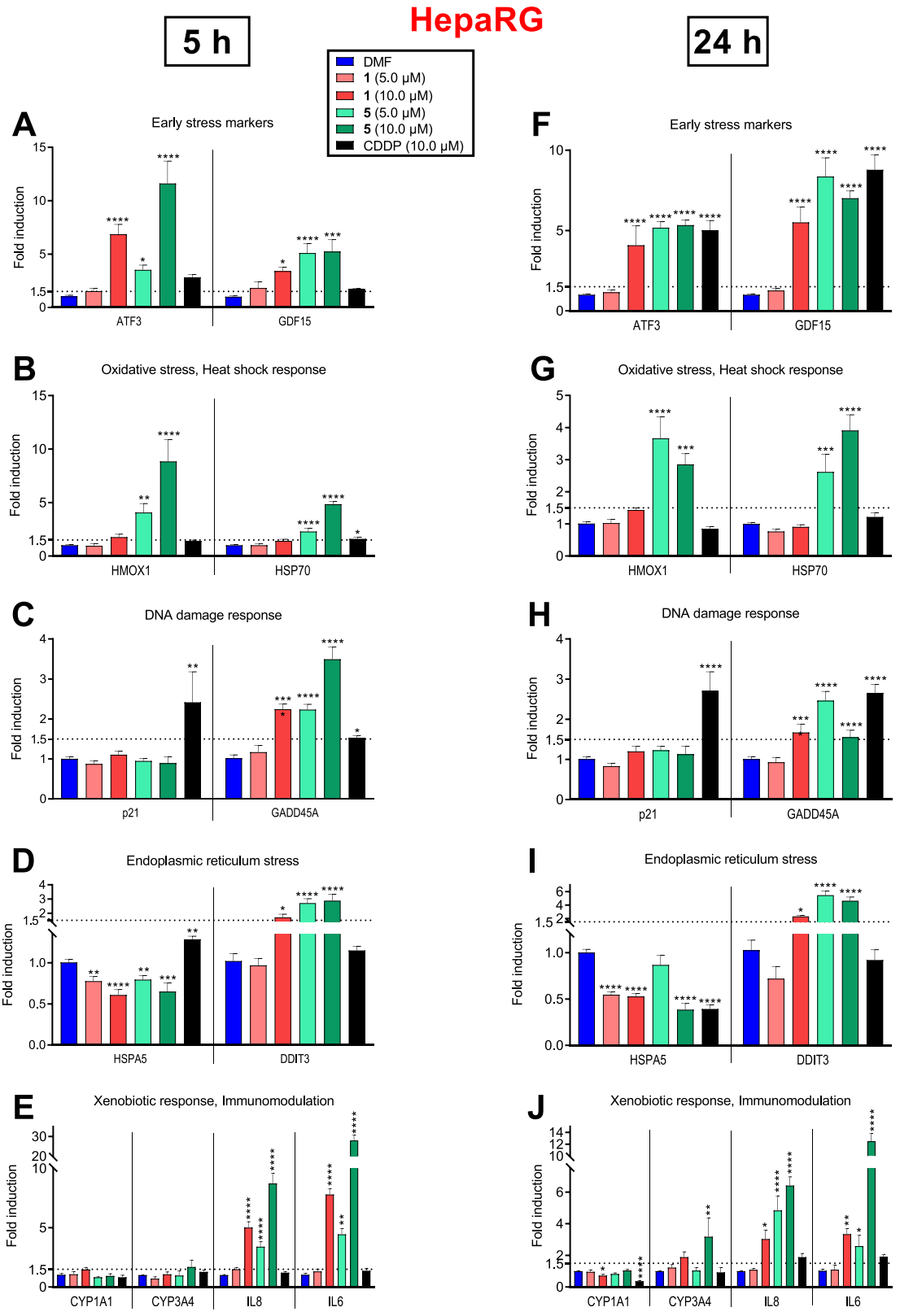

Fig. 9. Changes in the gene expression caused by complexes **1** and **5**, and cisplatin (CDDP). HepaRG cells were incubated with tested compounds at indicated concentrations or DMF (0.1 % v/v) only for 5 (**A**–**E**) and 24 h (**F**–**J**). The gene expression was evaluated by q-RT-PCR. The data are shown as the mean ± SEM; * indicates statistical significance ($p < 0.05$) compared with the DMF group; ** indicates statistical significance ($p < 0.01$) compared with the DMF group; *** indicates statistical significance ($p < 0.001$) compared with the DMF group; **** indicates statistical significance ($p < 0.0001$) compared with the DMF group.

optimize dosing (considering possible metabolism by AhR-induced enzymes), and determine whether their novel mode of action indeed translates into improved outcomes with acceptable toxicity in whole organisms. If their *in vitro* profile holds true *in vivo*, these PAH-functionalized Ru and Os complexes could significantly broaden the metallotherapeutic arsenal against cancer.

3. Conclusion

The research presented in this study explores the development and characterization of novel ruthenium(II) and osmium(II) half-sandwich complexes with polycyclic aromatic hydrocarbons (PAH)-substituted Schiff bases. The novel complexes exhibit high antiproliferative activity against lung cancer cells, including a cisplatin-resistant line. The incorporation of PAH groups in the Schiff bases leads to enhanced DNA intercalation, contributing to the potent antiproliferative effects observed. Notably, these complexes induced cell death via mechanisms that diverge from traditional DNA cross-linking, involving cellular stress responses, oxidative damage, and mitochondrial dysfunction.

The cellular studies revealed that complexes **1** and **5** caused apoptosis primarily through ER stress pathways, including the upregulation of stress-related genes like DDIT3 and ATF3. The compounds were also observed to induce mitochondrial membrane depolarization, a hallmark of early apoptosis, and increase mitochondrial mass, possibly as a compensatory mechanism. These findings suggest that the Ru and Os complexes engage multiple cellular stress pathways, including proteotoxicity, oxidative stress, and mitochondrial dysfunction, contributing to their unconventional anticancer efficacy. In comparison with cisplatin, which primarily activates DNA damage response pathways, the Ru and Os complexes display a distinct mode of action. They do not significantly activate inflammatory cytokines in cancer cells, an advantage that could reduce pro-tumour inflammation, making these complexes a promising alternative to cisplatin. Moreover, the potential for overcoming platinum resistance by targeting alternative stress pathways provides an exciting avenue for the development of more effective anticancer drugs. These findings pave the way for further preclinical and clinical investigations aimed at developing these complexes as viable alternatives to current chemotherapy options. The ability to bypass cisplatin resistance while minimizing inflammation could enhance the therapeutic outcomes for patients suffering from resistant forms of cancer, particularly lung cancer.

4. Experimental section

4.1. Materials

Chemicals ($RuCl_3{\cdot}xH_2O$, $RhCl_3{\cdot}xH_2O$, $OsCl_3{\cdot}xH_2O$, $IrCl_3{\cdot}xH_2O$, 1,2,3,4,5-pentamethylcyclopenta-1,3-diene (HCp*), 4-methyl-1-(1-methylethyl)-1,3-cyclohexadiene (α-terpinen), NH_4PF_6, KPF_6, $MgSO_4$, ethane-1,2-diamin, naphthalene-2-carbaldehyde, anthracene-9-carbaldehyde, phenanthrene-9-carbaldehyde, pyrene-1-carbaldehyde, cisplatin, phosphate-buffered saline (PBS; powder), β-nicotinamide adenine dinucleotide reduced disodium salt (NADH), β-nicotinamide adenine dinucleotide hydrate (NAD^+)), solvents (methanol, diethyl ether, dichloromethane (DCM), n-hexane, acetic acid) and deuterated NMR solvents ($CDCl_3$, C_6D_6, DMSO-d_6, D_2O, DMF-d_7) were supplied by Merck Life Science (Prague, Czech Republic), VWR International (Stříbrná Skalice, Czech Republic), Lach-Ner (Neratovice, Czech Republic) and Chemstar Czech Republic (Plzeň, Czech Republic). The chemicals and solvents were used as received.

Cell culture media and their supplements [foetal bovine serum (FBS), antibiotics, non-essential amino acids (NEAA)] were purchase from Biosera (Nuaille, France), anti-microbial agent Normocin was obtained from InvivoGen (San Diego, CA, USA). Collagenase I and Histopaque® 1077 were purchased from Merck (Darmstadt, Germany). A Cell Counting Kit 8 (CCK-8) was obtained from Abcam (Cambridge, UK). Vitrogel was obtained from InvivoGen. A Live/Dead Cell Imaging Kit and LIVE/DEAD Fixable Violet Dead Cell Stain Kit were obtained from Invitrogen (Eugene, OR, USA). An ApoflowEx FITC kit was produced by Exbio (Prague, Czech Republic). Cytotoxicity Detection KitPLUS and Universal Probe Library probes were obtained from Roche (Mannheim, Germany). TaqMan™ Gene Expression Assays were produced by Thermo Fisher Scientific (Waltham, MA, USA); the Kapa Probe Fast One-Step reaction mixture was purchased from Kapa Biosystems Pty (Cape Town, South Africa); and reference gene qPCR assays were obtained from Generi Biotech (Hradec Králové, Czech Republic).

The starting dinuclear complexes $[Ru(\mu\text{-}Cl)(\eta^6\text{-pcym})Cl]_2$ [48,49], $[Rh(\mu\text{-}Cl)(\eta^5\text{-Cp*})Cl]_2$ [49,50], $[Os(\mu\text{-}Cl)(\eta^6\text{-pcym})Cl]_2$ [51,52], and $[Ir(\mu\text{-}Cl)(\eta^5\text{-Cp*})Cl]_2$ [49,50] have been previously reported in the literature and were prepared using the Monowave 300 (Anton Paar) microwave reactor. Complex $[Ru(\eta^6\text{-pcym})Cl(en)]PF_6$ (**0**) was prepared as formerly reported in the literature [21].

4.2. Synthesis of organic compounds L1–L4

Ethane-1,2-diamine (1 mmol) was added to a suspension of a stoichiometric amount (2 mmol) of the aldehyde of the corresponding polycyclic aromatic hydrocarbon in 10 mL of methanol. The reaction mixture is acidified with four drops of acetic acid and then heated in a microwave reactor at 60 °C for 3 min. The resulting organic compounds (L1–L4) were filtered off, washed with cold methanol, and dried at 50 °C.

N,N′-bis [(*E*)-naphthalen-2-ylmethylidene]ethane-1,2-diamine (L1): Yield: 85 %. CHN analysis (%): calcd. for $C_{24}H_{20}N_2$: C, 85.7; H, 6.0; N, 8.3 %; found: C, 86.1; H, 6.2; N, 8.2 %. ^{1}H NMR (400 MHz, $CDCl_3$, 298 K, ppm): δ 8.46 (s, 2H), 7.97 (m, 4H), 7.84 (m, 6H), 7.49 (m, 4H), 4.08 (s, 4H).

N,N′-bis [(*E*)-anthracen-9-ylmethylidene]ethane-1,2-diamine (L2): Yield: 80 %. CHN analysis (%): calcd. for $C_{32}H_{24}N_2$: C, 88.0; H, 5.5; N, 6.4 %; found: C, 87.7; H, 5.4; N, 6.5 %. ^{1}H NMR (400 MHz, C_6D_6, 298 K, ppm): δ 9.22 (s, 2H), 8.67 (d, $J = 8.6$ Hz, 4H), 8.13 (s, 2H), 7.72 (d, $J = 8.2$ Hz, 4H), 6.99 (m, 4H), 4.21 (s, 4H).

N,N′-bis [(*E*)-phenanthren-9-ylmethylidene]ethane-1,2-diamine (L3): Yield: 90 %. CHN analysis (%): calcd. for $C_{32}H_{24}N_2$: C, 88.0; H, 5.5; N, 6.4 %; found: C, 87.9; H, 5.3; N, 6.2 %. ^{1}H NMR (400 MHz, $CDCl_3$, 298 K, ppm): δ 8.99 (s, 2H), 8.92 (d, $J = 8.2$ Hz, 2H), 8.67 (m, 4H), 8.08 (s, 2H), 7.88 (d, $J = 7.8$ Hz, 2H), 7.68 (d, $J = 7.6$ Hz, 2H), 7.59 (q, $J = 8.3$ Hz, 4H), 7.40 (t, $J = 7.6$ Hz, 2H), 4.26 (s, 4H).

N,N′-bis [(*E*)-pyren-1-ylmethylidene]ethane-1,2-diamine (L4): Yield: 85 %. CHN analysis (%): calcd. for $C_{36}H_{24}N_2$: C, 89.2; H, 5.0; N, 5.8 %; found: C, 89.0; H, 5.3; N, 5.6 %. ^{1}H NMR (400 MHz, $CDCl_3$, 298 K, ppm): δ 9.33 (s, 2H), 8.68 (d, $J = 9.4$ Hz, 2H), 8.52 (d, $J = 8.2$ Hz, 2H), 8.16 (d, $J = 8.2$ Hz, 4H), 8.01 (m, 8H), 7.79 (d, $J = 9.4$ Hz, 2H), 4.36 (s, 4H).

4.3. Synthesis of complexes

0.05 mmol of dimers $[M(\mu\text{-}Cl)(\eta^6\text{-pcym})Cl]_2$ (M = Ru for **1**–**4** or Os for **5**–**8**) or $[M(\mu\text{-}Cl)(\eta^5\text{-Cp*})Cl]_2$ (M = Rh for **9**–**12** or Ir for **13**–**16**) were suspended in MeOH (5 mL) in a microwave reaction vial, and 0.15 mmol of en-based Schiff base L1 (for **1**, **5**, **9** and **13**), L2 (for **2**, **6**, **10** and **14**), L3 (for **3**, **7**, **11** and **15**) or L4 (for **4**, **8**, **12** and **16**) was added. The reaction mixtures were heated in a microwave reactor (1 min, 100 °C), cooled to room temperature (r.t.), and filtered. After that, NH_4PF_6 or KPF_6 (0.25 mmol) was added to these solutions and these mixtures were stirred (r.t., 15 min). A portion of the MeOH was evaporated under a stream of nitrogen until complexes **1**–**16** precipitated. The products were removed and re-dissolved in 3 mL of DCM. An equal volume of water was added to this solution and the resulting mixture was shaken thoroughly. After separation of the DCM phase, this solution was dried by the addition of $MgSO_4$ and after filtration the filtrate was concentrated (nitrogen gas) to *ca.* 1 mL volume. Subsequent addition of *n*-hexane (*ca.* 5 mL) led to the formation of the solid product (**1**–**16**).

Products were washed (3 × 2 mL of cold diethyl ether) and dried overnight at 50 °C. Complexes are stable at r.t. and do not require special storage conditions.

Alternatively, 0.05 mmol of a dimer was suspended in 2 mL of MeOH in a microwave reaction vial, and 0.105 mmol of appropriate en-based Schiff base was added. The mixtures were heated in a microwave reactor (1 min ramp to 100 °C, 2 min isothermal hold, and cooling to 45 °C). After that, NH_4PF_6 (0.25 mmol) was added to these solutions and these mixtures were stirred (r.t., 10 min). The resulting yellow solids were filtered and washed three times with 1 mL of MeOH, 1 mL of cold diethyl ether, and dried in a desiccator under reduced pressure.

[Ru(η^6-pcym)Cl(L1)]PF_6 (**1**): Yield: 85 %. CHN analysis (%): calcd. for $C_{34}H_{34}N_2ClF_6PRu$: C, 54.3; H, 4.6; N, 3.7 %; found: C, 54.1; H, 4.3; N, 3.6 %. ^{1}H NMR (400 MHz, DMSO-d_6, 298 K, ppm): δ 9.37 (s, 2H), 8.77 (s, 2H), 8.48 (d, J = 8.6 Hz, 2H), 8.21 (d, J = 8.6 Hz, 2H), 8.10 (m, 4H), 7.72 (m, 4H), 4.89 (d, J = 6.1 Hz, 2H), 4.68 (d, J = 6.1 Hz, 2H), 4.07 (m, 2H), 3.74 (m, 2H), 2.63 (sep, J = 6.9 Hz, 1H), 2.07 (s, 3H), 1.04 (d, J = 6.9 Hz, 6H). ESI+ MS (MeOH, *m/z*): 571.3 (571.2 calcd. for {[Ru(L1)(pcym)]–H^+}$^+$; 65 %), 607.2 (607.1 calcd. for [RuCl(L1)(pcym)]$^+$; 100 %).

[Ru(η^6-pcym)Cl(L2)]PF_6 (**2**): Yield: 75 %. CHN analysis (%): calcd. for $C_{42}H_{38}N_2ClF_6PRu$: C, 59.2; H, 4.5; N, 3.3 %; found: C, 59.1; H, 4.2; N, 2.9 %. ^{1}H NMR (400 MHz, DMSO-d_6, 298 K, ppm): δ 10.14 (s, 2H), 8.93 (bs, 2H), 8.47 (d, J = 8.6 Hz, 1H), 8.37 (d, J = 8.6 Hz, 1H), 8.22 (m, 6H), 7.65 (m, 8H), 4.35 (bs, 4H), 4.11 (d, J = 6.3 Hz, 1H), 3.63 (d, J = 6.3 Hz, 1H), 2.29 (d, J = 5.9 Hz, 1H), 1.97 (d, J = 5.9 Hz, 1H), 1.86/1.49 (2 × sep, J = 6.8 Hz, 1H), 1.60/1.23 (2 × s, 3H), 0.58/–0.06 (2 × d, J = 6.6 Hz, 6H). ESI+ MS (MeOH, *m/z*): 671.1 (671.2 calcd. for {[Ru(L2)(pcym)]–H^+}$^+$; 5 %), 707.1 (707.2 calcd. for [RuCl(L2)(pcym)]$^+$; 100 %).

[Ru(η^6-pcym)Cl(L3)]PF_6 (**3**): Yield: 70 %. CHN analysis (%): calcd. for $C_{42}H_{38}N_2ClF_6PRu$: C, 59.2; H, 4.5; N, 3.3 %; found: C, 58.8; H, 4.4; N, 3.0 %. ^{1}H NMR (400 MHz, DMSO-d_6, 298 K, ppm): δ 9.78 (s, 2H), 9.01 (m, 6H), 8.45 (bs, 2H), 8.07 (d, J = 7.8 Hz, 2H), 7.87 (m, 8H), 4.34 (bs, 4H), 4.24 (bs, 2H), 3.91 (bs, 2H), 2.39 (sep, J = 7.0 Hz, 1H), 1.76 (s, 3H), 0.78 (d, J = 6.9 Hz, 6H). ESI+ MS (MeOH, *m/z*): 671.1 (671.2 calcd. for {[Ru(L3)(pcym)]–H^+}$^+$; 5 %), 707.2 (707.2 calcd. for [RuCl(L3)(pcym)]$^+$; 100 %).

[Ru(η^6-pcym)Cl(L4)]PF_6 (**4**): Yield: 80 %. CHN analysis (%): calcd. for $C_{46}H_{38}N_2ClF_6PRu$: C, 61.4; H, 4.3; N, 3.1 %; found: C, 61.1; H, 4.0; N, 2.9 %. ^{1}H NMR (400 MHz, DMSO-d_6, 298 K, ppm): δ 10.12 (s, 2H), 9.20 (d, J = 8.0 Hz, 2H), 8.71 (d, J = 9.2 Hz, 2H), 8.45 (m, 12H), 8.20 (t, J = 9.2 Hz, 2H), 4.40 (m, 4H), 4.10 (bs, 2H), 4.00 (m, 2H), 2.51 (s, 1H), 1.91 (s, 3H), 0.85 (d, J = 6.9 Hz, 6H). ESI+ MS (MeOH, *m/z*): 719.1 (719.3 calcd. for {[Ru(L4)(pcym)]–H^+}$^+$; 15 %), 755.2 (755.2 calcd. for [RuCl(L4)(pcym)]$^+$; 100 %).

[Os(η^6-pcym)Cl(L1)]PF_6 (**5**): Yield: 90 %. CHN analysis (%): calcd. for $C_{34}H_{34}N_2ClF_6OsP$: C, 48.5; H, 4.1; N, 3.3 %; found: C, 48.2; H, 4.5; N, 3.0 %. ^{1}H NMR (400 MHz, DMSO-d_6, 298 K, ppm): δ 9.38 (s, 2H), 8.69 (s, 2H), 8.35 (d, J = 8.6 Hz, 2H), 8.17 (d, J = 8.6 Hz, 2H), 8.08 (d, J = 8.2 Hz, 4H), 7.71 (m, 4H), 5.14 (d, J = 5.6 Hz, 2H), 4.83 (d, J = 5.6 Hz, 2H), 4.05 (bs, 2H), 3.86 (bs, 2H), 2.54 (sep, J = 6.9 Hz, 1H), 2.08 (s, 3H), 1.04 (d, J = 6.9 Hz, 6H). ESI+ MS (MeOH, *m/z*): 661.2 (661.2 calcd. for {[Os(L1)(pcym)]–H^+}$^+$; 85 %), 697.1 (697.1 calcd. for [OsCl(L1)(pcym)]$^+$; 100 %).

[Os(η^6-pcym)Cl(L2)]PF_6 (**6**): Yield: 75 %. CHN analysis (%): calcd. for $C_{42}H_{38}N_2ClF_6OsO$: C, 53.6; H, 4.1; N, 3.0 %; found: C, 53.7; H, 3.9; N, 2.8 %. ^{1}H NMR (400 MHz, DMSO-d_6, 298 K, ppm): δ 10.24 (s, 2H), 8.92 (bs, 2H), 8.40 (d, J = 8.6 Hz, 2H), 8.27 (m, 4H), 8.16 (t, J = 8.8 Hz, 2H), 7.64 (m, 8H), 4.45 (m, 5H), 3.96 (d, J = 9.4 Hz, 1H), 2.20 (d, J = 9.4 Hz, 1H), 1.88/1.34 (2 × bs, 1H), 1.80 (d, J = 14.8 Hz, 1H), 0.61 (m, 6H), −0.03 (bs, 3H). ESI+ MS (MeOH, *m/z*): 761.2 (761.2 calcd. for {[Os(L2)(pcym)]–H^+}$^+$; 25 %), 797.2 (797.2 calcd. for [OsCl(L2)(pcym)]$^+$; 100 %).

[Os(η^6-pcym)Cl(L3)]PF_6 (**7**): Yield: 85 %. CHN analysis (%): calcd. for $C_{42}H_{38}N_2ClF_6OsP$: C, 53.6; H, 4.1; N, 3.0 %; found: C, 53.9; H, 3.7; N, 2.9 %. ^{1}H NMR (400 MHz, DMSO-d_6, 298 K, ppm): δ 9.78 (s, 2H), 9.04 (d, J = 8.2 Hz, 2H), 8.97 (d, J = 8.2 Hz, 2H), 8.87 (s, 2H), 8.38 (m, 2H), 8.04 (d, J = 8.0 Hz, 2H), 7.85 (m, 8H), 4.34 (bs, 4H), 4.05 (m, 4H), 2.34 (bs, 1H), 1.80 (s, 3H), 0.78 (d, J = 6.9 Hz, 6H). ESI+ MS (MeOH, *m/z*): 761.2 (761.3 calcd. for {[Os(L3)(pcym)]–H^+}$^+$; 5 %), 797.2 (797.2 calcd. for [OsCl(L3)(pcym)]$^+$; 100 %).

[Os(η^6-pcym)Cl(L4)]PF_6 (**8**): Yield: 70 %. CHN analysis (%): calcd. for $C_{46}H_{38}N_2ClF_6OsP$: C, 58.8; H, 3.9; N, 2.8 %; found: C, 58.9; H, 3.7; N, 2.5 %. ^{1}H NMR (400 MHz, DMSO-d_6, 298 K, ppm): δ 10.12 (s), 10.06 (s), 9.18 (d, J = 8.2 Hz), 9.08 (d, J = 7.8 Hz), 8.66 (d, J = 9.0 Hz), 8.40 (m), 5.79 (d, J = 5.5 Hz), 5.46 (d, J = 5.5 Hz), 5.31 (d, J = 5.5 Hz), 5.04 (d, J = 5.5 Hz), 4.65 (bs), 4.41 (bs), 4.28 (bs), 4.13 (bs), 4.00 (bs), 3.66 (bs), 2.78 (sep, J = 6.7 Hz), 3.18 (s), 1.97 (s), 1.23 (d, J = 7.0 Hz), 0.88 (d, J = 6.7 Hz). ESI+ MS (MeOH, *m/z*): 809.3 (809.3 calcd. for {[Os(L4)(pcym)]–H^+}$^+$; 20 %), 845.2 (845.2 calcd. for [OsCl(L4)(pcym)]$^+$; 100 %).

[Rh(η^5-Cp*)Cl(L1)]PF_6 (**9**): Yield: 95 %. CHN analysis (%): calcd. for $C_{34}H_{35}N_2ClF_6PRh$: C, 54.1; H, 4.7; N, 3.7 %; found: C 54.0; H 4.5; N, 3.3 %. ^{1}H NMR (400 MHz, DMSO-d_6, 298 K, ppm): δ 9.29 (s, 1H), 9.06 (s, 1H), 8.90 (s, 1H), 8.71 (dd, J = 8.6, 1.7 Hz, 1H), 8.57 (s, 1H), 8.20–8.06 (m, 6H), 7.98 (dd, J = 8.7, 1.7 Hz, 1H), 7.77–7.66 (m, 4H), 4.29–4.12 (m, 3H), 3.90–3.80 (m, 1H), 1.52 (s, 15H). ESI+ MS (MeOH, *m/z*): 573.1 (573.2 calcd. for {[Rh(Cp*)(L1)]–H^+}$^+$; 100 %), 609.1 (609.1 calcd. for [RhCl(Cp*)(L1)]$^+$; 70 %).

[Rh(η^5-Cp*)Cl(L2)]PF_6 (**10**): ESI+ MS (MeOH, *m/z*): 673.3 (673.2 calcd. for {[Rh(Cp*)(L2)]–H^+}$^+$; 40 %), 709.2 (709.2 calcd. for [RhCl(Cp*)(L2)]$^+$; 100 %).

[Rh(η^5-Cp*)Cl(L3)]PF_6 (**11**): ESI+ MS (MeOH, *m/z*): 673.3 (673.2 calcd. for {[Rh(Cp*)(L3)]–H^+}$^+$; 40 %), 709.2 (709.2 calcd. for [RhCl(Cp*)(L3)]$^+$; 100 %).

[Rh(η^5-Cp*)Cl(L4)]PF_6 (**12**): ESI+ MS (MeOH, *m/z*): 721.2 (721.2 calcd. for {[Rh(Cp*)(L4)]–H^+}$^+$; 15 %), 757.2 (757.2 calcd. for [RhCl(Cp*)(L4)]$^+$; 100 %).

[Ir(η^5-Cp*)Cl(L1)]PF_6 (**13**): Yield: 90 %. CHN analysis (%): calcd. for $C_{34}H_{35}N_2ClF_6IrP$: C, 48.4; H, 4.2; N, 3.3 %; found: C, 47.8; H, 4.0; N, 3.4 %. ^{1}H NMR (400 MHz, DMSO-d_6, 298 K, ppm): δ 9.38 (s, 1H), 8.99 (d, J = 14.5, 3.8 Hz, 2H), 8.58 (s, 1H), 8.58 (s, 1H), 8.20–8.04 (m, 6H), 7.98 (dd, J = 8.6, 1.8 Hz, 1H), 7.77–7.65 (m, 4H), 4.29–4.20 (m, 2H), 4.11–3.92 (m, 2H), 1.48 (s, 15H). ESI+ MS (MeOH, *m/z*): 663.2 (663.2 calcd. for {[Ir(Cp*)(L1)]–H^+}$^+$; 45 %), 699.1 (699.2 calcd. for [IrCl(Cp*)(L1)]$^+$; 100 %).

[Ir(η^5-Cp*)Cl(L2)]PF_6 (**14**): ESI+ MS (MeOH, *m/z*): 763.4 (763.3 calcd. for {[Ir(Cp*)(L2)]–H^+}$^+$; 20 %), 799.3 (799.2 calcd. for [IrCl(Cp*)(L2)]$^+$; 100 %).

[Ir(η^5-Cp*)Cl(L3)]PF_6 (**15**): ESI+ MS (MeOH, *m/z*): 763.4 (763.3 calcd. for {[Ir(Cp*)(L3)]–H^+}$^+$; 10 %), 799.3 (799.2 calcd. for [IrCl(Cp*)(L3)]$^+$; 100 %).

[Ir(η^5-Cp*)Cl(L4)]PF_6 (**16**): ESI+ MS (MeOH, *m/z*): 811.4 (811.3 calcd. for {[Ir(Cp*)(L4)]–H^+}$^+$; 30 %), 847.2 (847.2 calcd. for [IrCl(Cp*)(L4)]$^+$; 100 %).

4.4. General methods

Electrospray ionization mass spectrometry (ESI-MS; methanol solutions) was carried out with an LCQ Fleet ion trap spectrometer (Thermo Scientific; QualBrowser software, version 2.0.7) in the positive (ESI+) ionization mode. Elemental analysis was performed by a Flash 2000 CHNS Elemental Analyser (Thermo Scientific).

^{1}H NMR spectroscopy and ^{1}H–^{1}H COSY experiments were recorded using $CDCl_3$ or DMSO-d_6 solutions at 298 K on a Varian-400 spectrometer (400 MHz); COSY = correlation spectroscopy. ^{1}H spectra were calibrated against the residual signals of the used solvent (^{1}H at 7.26 ppm for $CDCl_3$, 7.16 for C_6D_6 and 2.50 ppm for DMSO-d_6). The splitting of proton resonances in the reported ^{1}H spectra is defined as s = singlet, d = doublet, t = triplet, m = multiplet and bs = broad signal.

Reversed-phase high-performance liquid chromatography (RP-

HPLC) coupled to ESI + MS was performed on the UHPLC-MS device (Dionex/Thermo Fisher Scientific) equipped with an Acclaim 120 (C18 stationary phase; 5 μm pore size, 120 Å, 2.1 × 50 mm). The mixture of MeCN (A) and 0.1 % formic acid in H_2O (B) was used as the mobile phase at the gradients of 20 % A ($t = 0$ min), 80 % A ($t = 15$ min), 80 % A ($t =$ 20 min), 20 % A ($t = 21$ min) and 20 % A ($t = 30$ min) over a 30 min period (0.4 mL min^{-1} flow rate). The detection wavelength was 254 nm.

4.5. Crystallography

Monocrystals suitable for a single-crystal X-ray analysis were prepared for Ru complexes **1**, **2** and **4**. Furthermore, several crystalline products obtained from the solutions of the Rh and Ir complexes (mother liquors, re-crystallized products) were tested and we were able to determine the crystal structures of the complexes with the cleaved Schiff base ligands **9′** and **13'**.

Data collection for single crystals of **1**, **3**, and **4** was performed using a Stoe StadiVari equipped with a Pilatus3R 300K hybrid pixed array detector (Dectris) and a microfocused X-ray source Xenocs Genics 3D Cu HF (Cu Kα). All the crystal structures were solved using SHELXT program [53] and refined by the full matrix least-squares procedure with SHELXL (version 2019/2) [54] in OLEX2 (version 1.5) [55]. The multi-scan absorption corrections were applied using the program Stoe LANA [56]. The molecular structures and packing diagram were drawn with MERCURY [57]. The crystal structure of compound **4** was previously published [28], but the completeness of the collected diffraction data was low, and the experiment was performed at ambient temperature, compared to 150 K in the redetermination presented here. The pcym ligand in structure **4** is disordered in two positions with occupancy factors of 0.61 (1) and 0.39 (1). The disordered pcym ligand was modeled using same fragment restraints and rigid body (RIGU) restraints. CCDC deposition numbers: 2450152 (for **1**), 2450153 (for **3**) and 2450154 (for **4**).

The data collection for the complexes with the cleaved Schiff base ligands **9′** and **13′** was done using an XtaLAB Synergy-I diffractometer with a HyPix3000 hybrid pixel array detector and microfocused PhotonJet-I X-ray source (Cu Kα). The data integration and multi-scan absorption corrections were applied using the program CrysAlisPro 1.171.40.82a [58]. The crystal structures of **9′** and **13′** were solved and refined using the same programs as in the case of **1**, **3**, and **4**. The quality of the crystals of was very poor leading to unsatisfactorily diffraction data and high R-values. Therefore, both crystal structures were submitted to CSD as database communications [59,60]. For **9'**, the [Rh(η^5-Cp*)Cl(en)]$^+$ cation was formerly reported [29].

4.6. Stability studies

The appropriate amount of the complexes for 1 mM solutions in 50 % DMSO-d_6/50 % D_2O (*v*/*v*) was dissolved in DMSO-d_6 (250 μL) and 250 μL of the phosphate-buffered saline (PBS) solution in D_2O was added (DMSO-d_6 was added due to low solubility of the complexes in water). ^{1}H NMR spectra were recorded at various time points ($t = 0$–24 h). The obtained spectra were calibrated against the residual signal of DMSO-d_6 (2.50 ppm). Analogical experiments were performed with an addition of an excess of NADH (5 molar equiv.), which was dissolved in 250 μL of the PBS solution in D_2O prior its addition to the complexes dissolved in 250 μL of DMSO-d_6.

4.7. Cell culture

The cytotoxic effects of the tested complexes were evaluated on the lung cell lines A549 and MOR, the cisplatin-resistant MOR/CPR, and MRC-5 (all obtained from ECACC, Salisbury, UK). MOR cells were cultured in RPMI 1640 medium, A549 cells in DMEM High glucose medium, and MRC-5 cell in EMEM supplemented by 1 % NEAA; all media were supplemented with 10 % fetal bovine serum (FBS), antibiotics (100 U/mL penicillin and 100 mg/mL streptomycin), and antimicrobial agent Normocin. The cells were kept at 37 °C in a humidified atmosphere containing 5 % CO_2. MOR/CPR cells were cultivated in the presence of 1 μg/mL CDDP, as recommended by the supplier. Cells were usually passaged twice a week, and their viability was checked by vital staining with trypan blue.

Human peripheral blood mononuclear cells (PBMCs) were isolated from the buffy coat prepared from whole blood of healthy volunteers at the Department of Transfusion & Tissue Medicine of the University Hospital Brno. The buffy coat was mixed with PBS (NaCl, 137 mM; KCl, 2.7 mM; Na_2HPO_4, 10 mM; KH_2PO_4, 1.8 mM; pH 7.4) at a ratio of 1:1 and subsequently transferred into a cuvette containing Histopaque® 1077 with half the volume of the buffy coat/PBS mixture. After centrifugation (at 500 *g*/30 min/r.t.), the layer containing the PBMCs was aspirated, transferred to a new cuvette, and washed twice with cold PBS (followed by centrifugation at 500 *g*/10 min/4 °C). The washed cells were resuspended in complete RPMI 1640 medium [containing 10 % FBS, antibiotics (100 U/mL penicillin and 100 mg/mL streptomycin), and Normocin] and counted.

4.8. In vitro 2D and 3D cytotoxicity testing

The effect of the tested compounds on cell viability was evaluated using a Cell Counting Kit 8 (CCK8) according to the manufacturer's manual. The test compounds were dissolved in DMF (the concentration of DMF did not exceed 0.1 % v/v in the presence of cells) and CDDP was used as the positive control. Floating PBMCs were seeded at a concentration of 5×10^4 cells/well in a 96-well plate. Adherent A549, MOR, MOR/CPR, and MRC-5 cells were seeded into 96-well plate at a density of 1×10^4 cells/well and allowed to adhere overnight. The next day, the cultivation medium was changed (MOR/CPR cell obtained medium without CDDP), and the tested complexes were added 2 h later. Cell viability was measured 72 h later, and the IC_{50} values (the concentrations of the tested compounds that caused a 50 % decrease of metabolic active cells in comparison with the number of untreated cells) were calculated according to four-parameter logistic (4 PL) analysis, excluding outstanding values (ROUT algorithms, Q = 5 %) in Prism 7.05 software (GraphPad Software, Inc., San Diego, CA, USA).

To evaluate the anti-cancer potential of the tested complexes in a 3D cell model, which is more closely related to real cancer than 2D models [61], spheroids formed from A549 cells were used. A549 cells resuspended in serum-free DMEM were seeded at a density of 16×10^3 cells/well into a 96-well U-shaped bottom microtitre plate with a low cell binding surface (Thermo Scientific, Roskilde, Denmark). After 4 days, the medium was exchanged for medium containing 10 % FBS, and the spheroids were cultivated for another 3 days. Then, the grown spheroids (diameter of 0.5–1.0 mm) were transferred to a 96-well plate with a flat bottom, which was covered with Vitrogel matrix, forming a wide U-shaped bed. During the transfer, the medium was exchanged. Complexes **1** and **5** and CDDP at concentrations corresponding to their IC_{50} values obtained from 2D experiments (i.e., 6 μM for **1**, 1.2 μM for **5**, and 10 μM for CDDP) were added after 2 h of acclimatization to the spheroids in a CO_2 incubator. After 3 days of incubation, the spheroids were stained with a Live/Dead Cell Imaging Kit containing calcein AM and BOBO-3 iodide dyes to distinguish live and dead cells. After 30 min of incubation in the dark at room temperature, the shape of the spheroids and the amount and distribution of dye were analyzed via confocal microscopy (Leica TSP SP 8). At least 3 spheroids were analyzed for each compound.

4.9. Cell cycle analysis

Flow cytometry was used to evaluate the number of cells in the particular phases of the cell cycle. The protocol was described previously [62]. The cells were seeded at 6 well plate at a concentration of 3×10^5 cells/well and treated complexes **1** and **5**, CDDP, and DMF only for 24 h

and 72 h. For 24 h, the concentrations corresponding to their 3 × and 1 × IC_{50} values obtained for 72 h incubation were used to achieve strong cellular response. On the other hand, for 72 h incubation, the concentrations corresponding to their 0.5 × and 1 × IC_{50} values obtained for 72 h incubation were used to evaluate the effect of level of tested compounds. The cells were washed in cold PBS and fixed by low-speed vortexing in 70 % (v/v) cold ethanol at 4 °C overnight. Next, cells were stained by 100 μL Vindel solution (propidium iodide, RNase) for 20 min at RT and analyzed by flow cytometer Amnis CellStream (Luminex, USA). A minimum of 1.5 × 10^4 events were collected per sample for evaluation of the percentage of cells in G1, S, and G2/M phases of the cell cycle. The data were evaluated by CellStream Analysis 1.2.55 software. Experiments were performed in duplicate and in three independent repetitions.

4.10. Assessment of cell death

The assessment of cell death and apoptosis was determined by flow cytometry in the human lung cancer cell line A549. The staining protocol has been described previously [62] with minor modifications. The treated cells were stained with Annexin V Dyomics 647 dye (Exbio, Czech Republic; dilution 5 μL in 100 μL Annexin Binding Buffer) and LIVE/DEAD Fixable Violet Dead Cell Stain Kit (ThermoFisher Scientific, USA; dilution 1 μL in 100 μL Annexin Binding Buffer). After 15 min incubation at 37 °C in the dark, samples were centrifuged at 500×*g* for 5 min at room temperature. Detection was performed using Amnis CellStream (Luminex, USA) flow cytometer. Fluorescence was recorded using the appropriate filter sets for Annexin V Dyomics 642 (Ex/Em: 642/702 nm) and Live/Dead Violet (Ex/Em: 405/450 nm). Unstained and single-stained controls were used to adjust compensation and define the gating strategy. A minimum of 2 × 10^4 events excluding doublets and debris were subjected to analysis.

Analysis of cell death and apoptosis was performed using double staining on dot plots, with Annexin V Dyomics 642 on the x-axis and Live/Dead Violet on the y-axis. The dot plots were divided into four quadrants. Live cells (live cells/Annexin V negative; low left quadrant; LL), early apoptotic cells (live cells/Annexin V positive; low right quadrant; LR), late apoptotic cells (dead cells/Annexin V positive; upper right quadrant; UR), and necrotic/dead cells (dead cells/Annexin V negative; upper left quadrant; UL) were distinguished after double staining. The data were evaluated by CellStream Analysis 1.2.55 software. Experiments were performed in three independent repetitions.

4.11. Mitochondrial membrane potential studies

Changes in mitochondrial membrane potential ($\Delta\Psi_m$) after treatment by complexes **1** and **5**, CDDP, and DMF were assessed using the cationic dye tetramethylrhodamine methyl ester (TMRM) after 24 hours. This dye is permeable to cells that accumulate in active mitochondria. Reduced fluorescence indicates mitochondrial depolarization, which is a typical feature of early apoptosis. A549 cells were seeded into a 6-well cultivation plate at a concentration of 3 × 10^5 cells/well and allowed to adhere overnight. The cultivation medium was changed after 24 h and cells were treated. Following 24 h treatment, cells were collected and resuspended in culture medium containing TMRM at a final concentration of 100 nM. Cells were incubated with the dye at 37 °C for 30 min in the dark to allow adequate dye accumulation in polarized mitochondria. After incubation, cells were centrifuged at 500 *g* for 5 min at room temperature and samples were washed once with pre-warmed PBS buffer to remove excess dye and stained by LIVE/DEAD Fixable Violet Dead Cell Stain Kit (ThermoFisher Scientific, USA) at a dilution of 1:1000. After staining of viable and dead cells (15 min, 37 °C), the samples were washed, centrifuged at 500 *g* for 5 min at room temperature and resuspended in PBS for analysis. Flow cytometry analysis was performed using the flow cytometer Amnis CellStream (Luminex, USA). Carbonyl cyanide chlorophenylhydrazone (cccp; 50 μM) was used as a control for impaired mitochondrial membrane potential. Unstained cells and cells treated with carbocyanine iodide were used as controls for proper setting of flow cytometry analysis. A minimum of 1.5 × 10^4 live cells excluding doublets and debris were subjected to analysis. TMRM fluorescence was detected using the appropriate excitation/emission settings (Ex/Em: 548/574 nm). TMRM negative cells were gated as cells with $\Delta\Psi_m$, which is a typical feature of early apoptosis. The data were evaluated by CellStream Analysis 1.2.55 software. Experiments were performed in duplicate and in three independent repetitions.

4.12. Detection of amount and size of mitochondria

The amount and size of mitochondria were measured after staining cells with MitoTracker Green FM (Invitrogen, USA, cat. No. M46750). MitoTracker Green FM is a cell-permeant reagent that labels mitochondria in live cells. The cells were incubated with MitoTracker Green, allowing the dye to passively diffuse across the plasma membrane and accumulate in active mitochondria. Confocal microscopy was used to determine the localization and size of mitochondria. Meanwhile, flow cytometry analysis was employed to quantify the mitochondrial content.

Briefly, A549 cells (2 × 10^5 cells/well) were seeded during the logarithmic growth phase into a 10 % FBS medium on IBIDI chamber slides (cat. No. 80826) for confocal microscopy analysis. Similarly, A549 cells (1.4 × 10^5 cells/well) were plated on 6-well plates for flow cytometry and allowed them to adhere overnight at 37 °C with 5 % CO_2. The next day, the culture medium was replaced, and the tested compounds were added 2 h later at concentrations based on their IC_{50} values for 72 h. After the 72 h incubation, the culture medium was gently removed. MitoTracker Green FM solution diluted in medium (200 nM) was added to the cells and incubated at 37 °C for 30 min. In the end, the cells were imaged under a Leica SP8 confocal fluorescence microscope.

For flow cytometry, double staining was used to detect viability and mitochondrial content. First, cells were detached from the 6-well plate with trypsin (Gibco, USA, cat. No. 15400054), washed, and stained with the LIVE/DEAD Fixable Violet Dead Cell Stain Kit (ThermoFisher Scientific, USA, cat. No. L34964) for 15 min at 37 °C. The cells were then washed, stained with Mitotracker Green FM for 40 min at 37 °C, washed again, resuspended in 100 μL PBS, and finally analyzed using the Amnis CellStream flow cytometer (Luminex, USA). Fluorescence was recorded with the appropriate filter sets for MitoTracker Green FM (Ex/Em: 488/528 nm) and Live/Dead Violet (Ex/Em: 405/450 nm). Unstained controls were used to establish the gating strategy. A minimum of 2 × 10^4 events, excluding doublets and debris, were analyzed.

4.13. Expression of stress related genes

Changes in the gene expression of cellular stress markers were determined by quantitative real-time PCR (qRT–PCR) on human liver HepaRG™ (Biopredic, Rennes, France) and A549 cells. HepaRG™ were differentiated in 24-well plates as described previously [63], with minor changes. After differentiation, the cells were exposed to **1**, **5**, or CDDP in medium without the differentiating agent (2 % DMSO) for 5 or 24 h. Cytotoxicity was tested after 24 h with the Cytotoxicity Detection Kit^{PLUS}, according to the manufacturer's instructions. A549 cell were seeded as described above (chapter 4.8). Total RNA was isolated, and qRT−PCR was performed with primers, Universal Probe Library probes or TaqMan™ Gene Expression Assays, as described recently [63], with minor changes. The amplifications were carried out in 10 μL of Kapa Probe Fast One-Step reaction mixture containing 1 μL of the sample. Reference gene qPCR assays were used for the housekeeping genes human β2-microglobulin (B2M; #3030) and hydroxymethylbilane synthase (HMBS; #3032). The Cp values of these two genes were averaged to serve as a reference, and the changes in relative gene expression were calculated based on the comparative threshold cycle method [64].

CRediT authorship contribution statement

Jan Hošek: Writing – review & editing, Writing – original draft, Visualization, Validation, Supervision, Resources, Project administration, Methodology, Investigation, Funding acquisition, Formal analysis, Data curation, Conceptualization. **Kamila Petrželová:** Investigation, Data curation. **Renata Héžová:** Writing – review & editing, Writing – original draft, Methodology, Investigation, Data curation. **Nicol Straková:** Writing – review & editing, Writing – original draft, Methodology, Investigation, Data curation. **Simona Kajabová:** Investigation. **Ivan Nemec:** Methodology, Investigation, Data curation. **Pavlína Šimečková:** Methodology, Investigation, Formal analysis. **Kateřina Pěnčíková:** Investigation, Data curation. **Josef Mašek:** Methodology, Investigation. **Ján Moncoľ:** Methodology, Investigation. **Pavel Štarha:** Writing – review & editing, Writing – original draft, Visualization, Validation, Supervision, Resources, Project administration, Methodology, Investigation, Funding acquisition, Formal analysis, Data curation, Conceptualization.

Funding sources

This work was supported by the Czech Health Research Council (AZV) of the Ministry of Health of the Czech Republic (NU22-08-00236). The single-crystal crystallography of this work was supported by the Slovak Agency for Research and Development under number APVV–23–0006 and the Agency for Science and Innovation of the Slovak Republic (project VEGA 1/0686/23).

Declaration of competing interest

The authors declare the following competing financial interest(s): J. H., I.N. and P.Š. have filed a patent application in the Czech Republic (PV 2023-360) and an international patent application (PCT/CZ2024/050060). The other authors declare that they have no known competing financial interests or personal relationships that could have appeared to influence the work reported in this paper.

Acknowledgements

The authors also thank Mrs. Pavla Richterová for performing elemental analysis, Mr. Lukáš Masaryk for the synthesis of the studied compounds and his help with their analysis, and Mrs. Jovana Lisičić for her help with cytotoxicity determination.

Appendix A. Supplementary data

Supplementary data to this article can be found online at https://doi.org/10.1016/j.ejmech.2025.117970.

Data availability

Data will be made available on request.

References

[1] C.M. Rudin, E. Brambilla, C. Faivre-Finn, J. Sage, Small-cell lung cancer, Nat. Rev. Dis. Primers 7 (2021) 3, https://doi.org/10.1038/s41572-020-00235-0.
[2] A.S. Jain, A. Prasad, S. Pradeep, C. Dharmashekar, R.R. Achar, S. Ekaterina, S. Victor, R.G. Amachawadi, S.K. Prasad, R. Pruthvish, A. Syed, C. Shivamallu, S. P. Kollur, Everything old is new again: drug repurposing approach for non-small cell lung cancer targeting MAPK signaling pathway, Front. Oncol. 11 (2021) 741326, https://doi.org/10.3389/fonc.2021.741326.
[3] https://gco.iarc.fr/(visitedon2023/10/16.
[4] R.L. Siegel, K.D. Miller, N.S. Wagle, A. Jemal, Cancer statistics, CA Cancer J. Clin. 73 (2023) 17–48, https://doi.org/10.3322/caac.21763, 2023.
[5] A.G. Nicholson, M.S. Tsao, M.B. Beasley, A.C. Borczuk, E. Brambilla, W.A. Cooper, S. Dacic, D. Jain, K.M. Kerr, S. Lantuejoul, M. Noguchi, M. Papotti, N. Rekhtman, G. Scagliotti, P. van Schil, L. Sholl, Y. Yatabe, A. Yoshida, W.D. Travis, The 2021 WHO classification of lung tumors: impact of advances since 2015, J. Thorac. Oncol. 17 (2022) 362–387, https://doi.org/10.1016/j.jtho.2021.11.003.
[6] M. Wang, R.S. Herbst, C. Boshoff, Toward personalized treatment approaches for non-small-cell lung cancer, Nat. Med. 27 (2021) 1345–1356, https://doi.org/10.1038/s41591-021-01450-2.
[7] S. Ghosh, Cisplatin: the first metal based anticancer drug, Bioorg. Chem. 88 (2019) 102925, https://doi.org/10.1016/j.bioorg.2019.102925.
[8] A. Sigel, H. Sigel, E. Freisinger, R.K.O. Sigel (Eds.), Metallo-Drugs: Development and Action of Anticancer Agents. Metal Ions in Life Sciences Book 18, 1 ed., De Gruyter, 2018.
[9] B. Rosenberg, L. Van Camp, T. Krigas, Inhibition of cell division in *Escherichia coli* by electrolysis products from a platinum electrode, Nature 205 (1965) 698–699, https://doi.org/10.1038/205698a0.
[10] J.R. Durig, J. Danneman, W.D. Behnke, E.E. Mercer, The induction of filamentous growth in *Escherichia coli* by ruthenium and palladium complexes, Chem. Biol. Interact. 13 (1976) 287–294, https://doi.org/10.1016/0009-2797(76)90081-8.
[11] E. Alessio, L. Messori, NAMI-A and KP1019/1339, two iconic ruthenium anticancer drug candidates Face-to-Face: a case story in medicinal inorganic chemistry, Molecules 24 (2019) 1995, https://doi.org/10.3390/molecules24101995.
[12] R. Trondl, P. Heffeter, C.R. Kowol, M.A. Jakupec, W. Berger, B.K. Keppler, NKP-1339, the first ruthenium-based anticancer drug on the edge to clinical application, Chem. Sci. 5 (2014) 2925–2932, https://doi.org/10.1039/C3SC53243G.
[13] S. Monro, K.L. Colón, H. Yin, J. Roque 3rd, P. Konda, S. Gujar, R.P. Thummel, L. Lilge, C.G. Cameron, S.A. McFarland, Transition metal complexes and photodynamic therapy from a tumor-centered approach: challenges, opportunities, and highlights from the development of TLD1433, Chem. Rev. 119 (2019) 797–828, https://doi.org/10.1021/acs.chemrev.8b00211.
[14] S.M. Meier-Menches, C. Gerner, W. Berger, C.G. Hartinger, B.K. Keppler, Structure-activity relationships for ruthenium and osmium anticancer agents - towards clinical development, Chem. Soc. Rev. 47 (2018) 909–928, https://doi.org/10.1039/C7CS00332C.
[15] A. Dorcier, W.H. Ang, S. Bolaño, L. Gonsalvi, L. Juillerat-Jeannerat, G. Laurenczy, M. Peruzzini, A.D. Phillips, F. Zanobini, P.J. Dyson, In vitro evaluation of rhodium and osmium RAPTA analogues: the case for organometallic anticancer drugs not based on ruthenium, Organometallics 25 (2006) 4090–4096, https://doi.org/10.1021/om060394o.
[16] S. Schäfer, I. Ott, R. Gust, W.S. Sheldrick, Influence of the polypyridyl (pp) ligand size on the DNA binding properties, cytotoxicity and cellular uptake of organoruthenium(II) complexes of the type $[(\eta^6\text{-}C_6Me_6)Ru(L)(pp)]^{n+}$ [L = Cl, n = 1; L = $(NH_2)_2CS$, n = 2], Eur. J. Inorg. Chem. (2007) 3034–3046, https://doi.org/10.1002/ejic.200700206.
[17] C.H. Leung, H.J. Zhong, D.S.H. Chan, D.L. Ma, Bioactive iridium and rhodium complexes as therapeutic agents, Coord. Chem. Rev. 257 (2013) 1764–1776, https://doi.org/10.1016/j.ccr.2013.01.034.
[18] K. Máliková, L. Masaryk, P. Štarha, Anticancer half-sandwich rhodium(III) complexes, INORGA 9 (2021) 26, https://doi.org/10.3390/inorganics9040026.
[19] D.L. Ma, C. Wu, K.J. Wu, C.H. Leung, Iridium(III) complexes targeting apoptotic cell death in cancer cells, Molecules 24 (2019) 2739, https://doi.org/10.3390/molecules24152739.
[20] P. Štarha, Anticancer iridium(III) cyclopentadienyl complexes, Inorg. Chem. Front. 12 (2025) 897–954, https://doi.org/10.1039/D4QI02472A.
[21] R.E. Morris, R.E. Aird, P. del Socorro Murdoch, H. Chen, J. Cummings, N. D. Hughes, S. Parsons, A. Parkin, G. Boyd, D.I. Jodrell, P.J. Sadler, Inhibition of cancer cell growth by ruthenium(II) arene complexes, J. Med. Chem. 44 (2001) 3616–3621, https://doi.org/10.1021/jm010051m.
[22] A.F.A. Peacock, A. Habtemariam, S.A. Moggach, A. Prescimone, S. Parsons, P. J. Sadler, Chloro half-sandwich osmium(II) complexes: influence of chelated N,N-ligands on hydrolysis, guanine binding, and cytotoxicity, Inorg. Chem. 46 (2007) 4049–4059, https://doi.org/10.1021/ic062350d.
[23] A. Wolfe, G.H. Shimer Jr., T. Meehan, Polycyclic aromatic hydrocarbons physically intercalate into duplex regions of denatured DNA, Biochemistry 26 (1987) 6392–6396, https://doi.org/10.1021/bi00394a013.
[24] S. Srivastava, R. Mishra, Some mercury(II) complexes with bidentate aromatic Schiff base ligands, J. Indian Chem. Soc. 72 (1995) 719–720.
[25] A.M. Costa, C. Jimeno, J. Gavenonis, P.J. Carroll, P.J. Walsh, Optimization of catalyst enantioselectivity and activity using achiral and meso ligands, J. Am. Chem. Soc. 124 (2002) 6929–6941, https://doi.org/10.1021/ja0166601.
[26] S. Lahlou, N. Bitit, J.-P. Desvergne, Syntheses and photoreactivity of new bisanthracenes incorporating one or two nitrogen atoms in the linkage, J. Chem. Res. 1998 (1998) 302–303, https://doi.org/10.1039/A708628H.
[27] D. Braun, R. Langendorf, I. Vitrigens, Synthesis and characterization of low molecular weight organic glasses, J. Prakt. Chem. 341 (1999) 128–137, https://doi.org/10.1002/(SICI)1521-3897(199902)341:2<128::AID-PRAC128>3.0.CO;2-M.
[28] D. Gopalakrishnan, S. Srinath, B. Baskar, N.S.P. Bhuvanesh, M. Ganeshpandian, Biological and catalytic evaluation of Ru(II)-p-cymene complexes of schiff base ligands: impact of ligand appended moiety on photo-induced DNA and protein cleavage, cytotoxicity and C-H activation, Appl. Organomet. Chem. 33 (2019) e4756, https://doi.org/10.1002/aoc.4756.
[29] G. García, G. Sánchez, I. Romero, I. Solano, M.D. Santana, G. López, Reactivity of $[\{\eta^5\text{-}C_5Me_5RhCl(\mu\text{-}Cl)\}_2]$ towards some potentially bidentate ligands, J. Organomet. Chem. 408 (1991) 241–246, https://doi.org/10.1016/0022-328X(91)86388-7.
[30] C.A. Riedl, L.S. Flocke, M. Hejl, A. Roller, M.H. Klose, M.A. Jakupec, W. Kandioller, B.K. Keppler, Introducing the 4-phenyl-1,2,3-triazole moiety as a versatile scaffold for the development of cytotoxic ruthenium(II) and osmium(II) arene

cyclometalates, Inorg. Chem. 56 (2017) 528–541, https://doi.org/10.1021/acs.inorgchem.6b02430.
[31] J. Hildebrandt, N. Häfner, D. Kritsch, H. Görls, M. Dürst, I.B. Runnebaum, W. Weigand, Highly cytotoxic osmium(II) compounds and their ruthenium(II) analogues targeting ovarian carcinoma cell lines and evading cisplatin resistance mechanisms, Int. J. Mol. Sci. 23 (2022) 4976, https://doi.org/10.3390/ijms23094976.
[32] J. Pracharova, V. Novohradsky, H. Kostrhunova, P. Štarha, Z. Trávníček, J. Kasparkova, V. Brabec, Half-sandwich Os(II) and Ru(II) bathophenanthroline complexes: anticancer drug candidates with unusual potency and a cellular activity profile in highly invasive triple-negative breast cancer cells, Dalton Trans. 47 (2018) 12197–12208, https://doi.org/10.1039/C8DT02236D.
[33] W.F. Schmid, R.O. John, G. Mühlgassner, P. Heffeter, M.A. Jakupec, M.S. Galanski, W. Berger, V.B. Arion, B.K. Keppler, Metal-based paullones as putative CDK inhibitors for antitumor chemotherapy, J. Med. Chem. 50 (2007) 6343–6355, https://doi.org/10.1021/jm701042w.
[34] I. Romero-Canelón, L. Salassa, P.J. Sadler, The contrasting activity of iodido versus chlorido ruthenium and osmium arene azo- and imino-pyridine anticancer complexes: control of cell selectivity, cross-resistance, p53 dependence, and apoptosis pathway, J. Med. Chem. 56 (2013) 1291–1300, https://doi.org/10.1021/jm3017442.
[35] P. Štarha, Z. Trávníček, J. Vančo, Z. Dvořák, Half-sandwich Ru(II) and Os(II) bathophenanthroline complexes containing a releasable dichloroacetato ligand, Molecules 23 (2018) 420, https://doi.org/10.3390/molecules23020420.
[36] J.D. Ly, D.R. Grubb, A. Lawen, The mitochondrial membrane potential ($\Delta\psi_m$) in apoptosis; an update, Apoptosis 8 (2003) 115–128, https://doi.org/10.1023/A:1022945107762.
[37] R.J. Mitchell, A.S. Gowda, A.G. Olivelli, A.J. Huckaba, S. Parkin, J.M. Unrine, V. Oza, J.S. Blackburn, F. Ladipo, D.K. Heidary, E.C. Glazer, Triarylphosphine-coordinated bipyridyl Ru(II) complexes induce mitochondrial dysfunction, Inorg. Chem. 62 (2023) 10940–10954, https://doi.org/10.1021/acs.inorgchem.3c00736.
[38] N.L. Wilke, H. Burmeister, C. Frias, I. Ott, A. Prokop, Ruthenium complex HB324 induces apoptosis via mitochondrial pathway with an upregulation of Harakiri and overcomes cisplatin resistance in neuroblastoma cells *in vitro*, Int. J. Mol. Sci. 24 (2023) 952, https://doi.org/10.3390/ijms24020952.
[39] J. Cervinka, A. Gobbo, L. Biancalana, L. Markova, V. Novohradsky, M. Guelfi, S. Zacchini, J. Kasparkova, V. Brabec, F. Marchetti, Ruthenium(II)–tris-pyrazolylmethane complexes inhibit cancer cell growth by disrupting mitochondrial calcium homeostasis, J. Med. Chem. 65 (2022) 10567–10587, https://doi.org/10.1021/acs.jmedchem.2c00722.
[40] S.H. van Rijt, I. Romero-Canelón, Y. Fu, S.D. Shnyder, P.J. Sadler, Cellular uptake and distribution of a potent organometallic anticancer drug candidate, KP1019, and its active metabolite KP1019-M1 in colorectal cancer cells, Metallomics 6 (2014) 1014–1022, https://doi.org/10.1039/C4MT00034J.
[41] Y. Gao, P. Dorn, S. Liu, H. Deng, S.R.R. Hall, R.-W. Peng, R.A. Schmid, T.M. Marti, Cisplatin-resistant A549 non-small cell lung cancer cells can be identified by increased mitochondrial mass and are sensitive to pemetrexed treatment, Cancer Cell Int. 19 (2019) 317, https://doi.org/10.1186/s12935-019-1037-1.
[42] R. Marullo, E. Werner, N. Degtyareva, B. Moore, G. Altavilla, S.S. Ramalingam, P. W. Doetsch, Cisplatin induces a mitochondrial-ROS response that contributes to cytotoxicity depending on mitochondrial redox status and bioenergetic functions, PLoS One 8 (2013) e81162, https://doi.org/10.1371/journal.pone.0081162.
[43] C. Licona, M. Spaety, A. Capuozzo, M. Ali, R. Santamaria, O. Armant, F. Delalande, A. Van Dorsselaer, S. Cianferani, J. Spencer, M. Pfeffer, G. Mellitzer, C. Gaiddon, A ruthenium anticancer compound interacts with histones and impacts differently on epigenetic and death pathways compared to cisplatin, Oncotarget 8 (2017) 2568–2584, https://doi.org/10.18632/oncotarget.13711.
[44] M.S. Alsaeedi, B.A. Babgi, M.H. Abdellattif, A. Jedidi, M.G. Humphrey, M. A. Hussien, DNA-binding capabilities and anticancer activities of ruthenium(II) cymene complexes with (poly)cyclic aromatic diamine ligands, Molecules 26 (2021) 76, https://doi.org/10.3390/molecules26010076.
[45] E. Kiss, E.H.M.M. Abdelwahab, A. Steib, E. Papp, Z. Torok, L. Jakab, G. Smuk, V. Sarosi, J.E. Pongracz, Cisplatin treatment induced interleukin 6 and 8 production alters lung adenocarcinoma cell migration in an oncogenic mutation dependent manner, Respir. Res. 21 (2020) 120, https://doi.org/10.1186/s12931-020-01389-x.
[46] J.K. Roberts, C.D. Moore, E.G. Romero, R.M. Ward, G.S. Yost, C.A. Reilly, Regulation of CYP3A genes by glucocorticoids in human lung cells, F1000Res 2 (2013) 173, https://doi.org/10.12688/f1000research.2-173.v2.
[47] D.W. Nebert, T.P. Dalton, A.B. Okey, F.J. Gonzalez, Role of aryl hydrocarbon receptor-mediated induction of the CYP1 enzymes in environmental toxicity and cancer, J. Biol. Chem. 279 (2004) 23847–23850, https://doi.org/10.1074/jbc.R400004200.1.
[48] M.A. Bennett, T.-N. Huang, T.W. Matheson, A.K. Smith, (η^6-Hexamethylbenzene) ruthenium complexes, Inorg. Synth. 21 (1982) 74, https://doi.org/10.1002/9780470132524.ch16.
[49] J. Tönnemann, J. Risse, Z. Grote, R. Scopelliti, K. Severin, Efficient and rapid synthesis of chlorido-bridged half-sandwich complexes of ruthenium, rhodium, and iridium by microwave heating, Eur. J. Inorg. Chem. (2013) 4558–4562, https://doi.org/10.1002/ejic.201300600.
[50] C. White, A. Yates, P.M. Maitlis, (η^5-Pentamethylcyclopentadienyl)rhodium and -iridium compounds, Inorg. Synth. 29 (1992) 228–234, https://doi.org/10.1002/9780470132609.ch53.
[51] T. Arthur, T.A. Stephenson, Synthesis of triple halide-bridged arene complexes of ruthenium(II) and osmium(II), J. Organomet. Chem. 208 (1981) 369–387, https://doi.org/10.1016/S0022-328X(00)86722-4.
[52] J.P.C. Coverdale, C. Sanchez-Cano, G.J. Clarkson, R. Soni, M. Wills, P.J. Sadler, Easy to synthesize, robust organo-osmium asymmetric transfer hydrogenation catalysts, Chem. Eur J. 21 (2015) 8043–8046, https://doi.org/10.1002/chem.201500534.
[53] G.M. Sheldrick, SHELXT - integrated space-group and crystal-structure determination, Acta Crystallogr. A71 (2015) 3–8, https://doi.org/10.1107/S2053273314026370.
[54] G.M. Sheldrick, Crystal structure refinement with SHELXL, Acta Crystallogr. C71 (2015) 3–8, https://doi.org/10.1107/S2053229614024218.
[55] O.V. Dolomanov, L.J. Bourhis, R.J. Gildea, J.A.K. Howard, H. Puschman, OLEX2: a complete structure solution, refinement and analysis program, J. Appl. Crystallogr. 42 (2008) 339–341, https://doi.org/10.1107/S0021889808042726.
[56] J. Koziskova, F. Hahn, J. Richter, J. Kozisek, Comparison of different absorption corrections on the model structure of tetrakis(μ_2-acetato)-diaqua-di-copper(II), Acta Chim. Slovaca 9 (2016) 136–140, https://doi.org/10.1515/acs-2016-0023.
[57] C.F. Macrae, I. Sovago, S.J. Cottrell, P.T.A. Galek, P. McCabe, E. Pidcock, M. Platings, G.P. Shields, J.S. Stevens, M. Towler, P.A. Wood, J. Appl. Crystallogr. 53 (2020) 226–235, https://doi.org/10.1107/S1600576719014092.
[58] Crysalispro 1.171.40.82a, Rigaku Oxford Diffraction, 2020.
[59] K. Petrzelova, I. Nemec, P. Starha, CCDC 2451058: experimental crystal structure determination. https://doi.org/10.5517/ccdc.csd.cc2n8jdw, 2025.
[60] K. Petrzelova, I. Nemec, P. Starha, CCDC 2451057: experimental crystal structure determination. https://doi.org/10.5517/ccdc.csd.cc2n8jcv, 2025.
[61] L.C. Kimlin, G. Casagrande, V.M. Virador, *In vitro* three-dimensional (3D) models in cancer research: an update, Mol. Carcinog. 52 (2013) 167–182, https://doi.org/10.1002/mc.21844.
[62] J. Hofmanová, J. Slavík, P. Ovesná, Z. Tylichová, J. Vondráček, N. Straková, A. H. Vaculová, M. Ciganek, A. Kozubík, L. Knopfová, J. Šmarda, M. Machala, Dietary fatty acids specifically modulate phospholipid pattern in colon cells with distinct differentiation capacities, Eur. J. Nutr. 56 (2017) 1493–1508, https://doi.org/10.1007/s00394-016-1196-y.
[63] P. Šimečková, F. Hubatka, J. Kotouček, P. Turánek Knötigová, J. Mašek, J. Slavík, O. Kováč, J. Neča, P. Kulich, D. Hrebík, J. Stráská, K. Pěnčíková, J. Procházková, P. Diviš, S. Macaulay, R. Mikulík, M. Raška, M. Machala, J. Turánek, Gadolinium labelled nanoliposomes as the platform for MRI theranostics: in vitro safety study in liver cells and macrophages, Sci. Rep. 10 (2020) 4780, https://doi.org/10.1038/s41598-020-60284-z.
[64] T.D. Schmittgen, K.J. Livak, Analyzing real-time PCR data by the comparative C(T) method, Nat. Protoc. 3 (2008) 1101–1108, https://doi.org/10.1038/nprot.2008.73.